AD-A032 732 MASSACHUSETTS INST OF TECH LEXINGTON LINCOLN LAB F/G 17/9
RADAR DETECTION OF THUNDERSTORM HAZARDS FOR AIR TRAFFIC CONTROL--ETC(U)
OCT 76 R K CRANE F19628-76-C-0002
UNCLASSIFIED ATC-67-VOL-1 FAA-RD-76-52-VOL-1 NL

1 OF 1
AD A032732

END
DATE FILMED
2-77

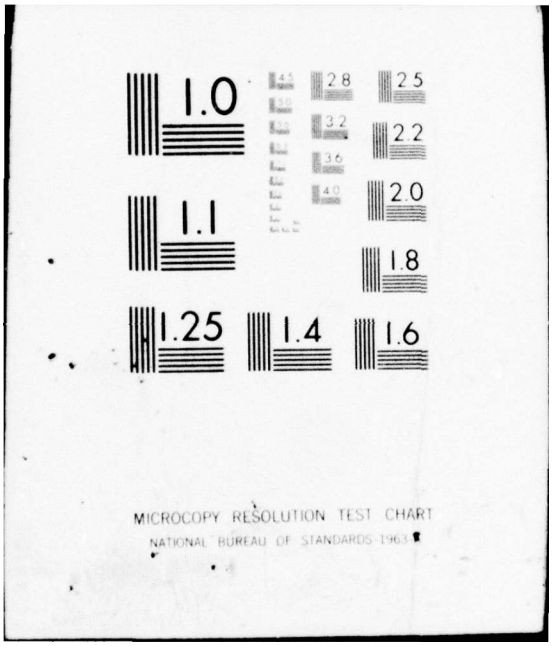
1.0
1.1
1.25
1.4
1.6
1.8
2.0
2.2
2.5
2.8
3.2
3.6
4.0
MICROCOPY RESOLUTION TEST CHART
NATIONAL BUREAU OF STANDARDS 1963

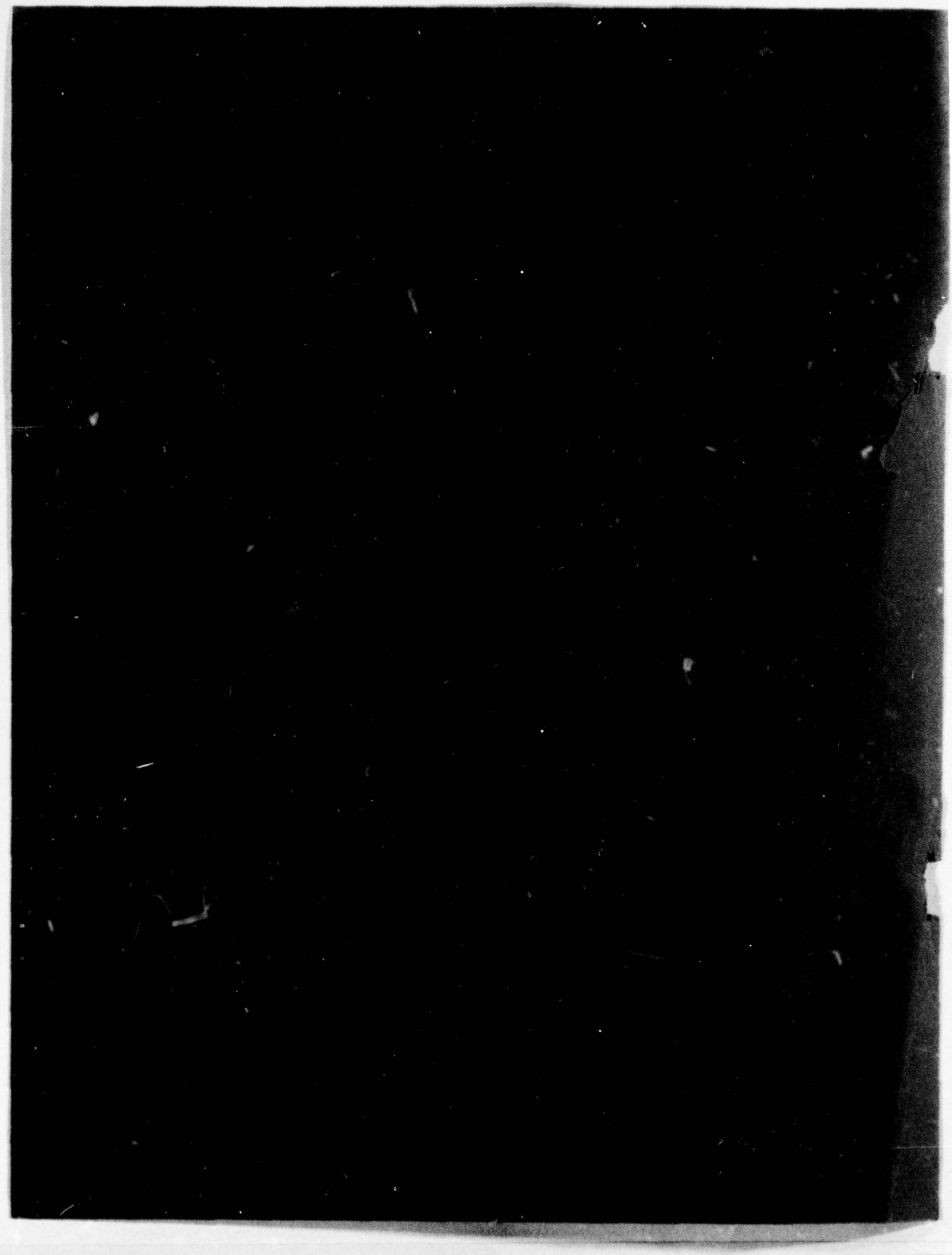

Technical Report Documentation Page

1. Report No.	2. Government Accession No.	3. Recipient's Catalog No.
(19) (18) FAA-RD-76-52-Vol-1		

4. Title and Subtitle

(6) Radar Detection of Thunderstorm Hazards for Air Traffic Control. Volume I. Storm Cell Detection.

5. Report Date

(11) 7 Oct 76

6. Performing Organization Code

7. Author(s)

(10) Robert K. Crane

(12) 69 p.

8. Performing Organization Report No.

(14) ATC-67-Vol-1

9. Performing Organization Name and Address

Massachusetts Institute of Technology
Lincoln Laboratory
P. O. Box 73
Lexington, Massachusetts 02173

10. Work Unit No. (TRAIS)

(15) F19628-76-C-0002,

11. Contract or Grant No.

DOT-FA74WAI-485,

12. Sponsoring Agency Name and Address

Department of Transportation
Federal Aviation Administration
Systems Research and Development Service
Washington, D.C. 20591

13. Type of Report and Period Covered

(9) Project Report.

14. Sponsoring Agency Code

15. Supplementary Notes

The work reported in this document was performed at Lincoln Laboratory, a center for research, operated by Massachusetts Institute of Technology under Air Force Contract F19628-76-C-0002.

16. Abstract

A procedure was developed to detect hazardous regions within thunderstorms using weather radar data. The procedure is based upon the hypothesis that convective turbulence occurs within 2-3 km of relative radar reflectivity maxima (cells). The hypothesis was tested using a limited set of simultaneous aircraft and radar data. Good agreement was found between the observed regions of convective turbulence and the cell locations determined by radar.

The viability of the hazard detection hypothesis as a basis for automatic warning and forecast depends upon the reliability of the cell detection and tracking algorithms. Analysis of precision radar data revealed that the cells are small in area extent, have a detection probability in excess of 0.9 using multiple radar scans, and are readily tracked for periods between 10 and 20 minutes.

The characteristics of radar systems for acquiring data to support cell detection, are discussed.

The role of Doppler spectral data is explored, and it is found that practical limitations on radar beamwidth hamper direct observation of turbulence on the scale size hazardous to aircraft.

17. Key Words		18. Distribution Statement
radar weather storm detection	cell detection cell tracking	Document is available to the public through the National Technical Information Service, Springfield, Virginia 22151.

19. Security Classif. (of this report)	20. Security Classif. (of this page)	21. No. of Pages	22. Price
Unclassified	Unclassified	60	

Form DOT F 1700.7 (8-72) Reproduction of completed page authorized

207650

TABLE OF CONTENTS

LIST OF ILLUSTRATIONS

LIST OF ILLUSTRATIONS (Cont'd)

LIST OF TABLES

1.0 INTRODUCTION

1.1 Program Objectives

The concept and plan for weather support for Air Traffic Control developed by Lincoln Laboratory [1]* documented the need for the detection and forecast of convective turbulence. Very short range (10-20 minute) forecasts are required to alert en route and terminal controllers to potential severe weather hazards to aircraft under their jurisdiction. Very short range forecasts of hazardous regions and their future movement would permit controllers to preplan for pilot-requested course deviations and to issue advisories where appropriate.

The objectives of the work reported herein were:

- Develop a procedure to detect hazardous regions within thunderstorms
- Determine the feasibility of providing 10-20 minute computer forecasts of the locations of the hazardous regions
- Define the minimum radar system characteristics required for hazard detection and forecast

This program was undertaken to provide the foundation for radar-related processing functions that comprise a significant fraction of any future weather support system for Air Traffic Control. Radar system designs to satisfy these functions are treated in Volume II.

1.2 Summary of Results

A procedure was developed to detect hazardous regions within thunderstorms. The procedure is based upon the hypothesis that convective turbulence within thunderstorms occurs within 2-3 km of localized increases or relative maxima of radar reflectivity called cells. This hazard detection hypothesis was tested with a small sample of data provided by the National Severe Storms Laboratory (NSSL). The NSSL data included both aircraft penetrations through thunderstorm regions and radar reflectivity maps for those regions. Good agreement was found between the locations of turbulent regions detected by the aircraft and the locations predicted using the hazard detection hypothesis.

*Number in brackets refers to references pp. 53-54.

The hazard detection hypothesis is viable only if the hazardous cells can be reliably detected and tracked. Analysis of precision radar data revealed that potentially hazardous cells can be reliably detected and that very short range forecasts are feasible. The precision weather radar data were obtained from the National Aeronautics and Space Administration (NASA) SPANDAR S-band radar at Wallops Island, Virginia. These data were processed to provide cell detection statistics and to investigate the feasibility of forecasting cell positions. Using a single azimuth scan of the antenna, the probability of cell detection ranged from 0.6 to 0.9 for reflectivity values from 35 dBz to greater than 60 dBz. The higher detection probabilities are for the higher reflectivity cells. Data from more than one scan are required to provide cell height and track information. For an operational system, more than three separate scans over a 6 to 8 minute interval would be used for cell detection and tracking which increases the detection probabilities to the range from 0.94 to 0.999. The missed cells are believed to be in the vicinity of other detected cells. Strategies to optimize hazard identification must be studied further.

The cell tracking analysis showed that the cells can be reliably tracked. The cells persisted for times ranging between 5 and 50 minutes. The longer durations correspond to higher cell reflectivity values and presumably to the more hazardous cells. For the cells studied, their half life or median lifetime was approximately 12 minutes.

The radar system characteristics required to reliably detect and track hazardous cells are listed in Table I. A number of radars currently in the FAA, National Weather Service (NWS) or U.S. Air Force inventories are capable of meeting these requirements. In all cases, additional data processing is required and restrictions must be placed both on their mode of operation and on the maximum distance to which they will be used. The modifications required to provide an adequate cell detection capability for terminal areas using the ASR radars in the FAA inventory are considered by Sussman [3]. These modifications do not compromise the ability of the radars to provide aircraft

surveillance. A recommended joint use radar to support the needs of the FAA and to provide data inputs to the other user agencies (NWS and Air Weather Service) is also discussed in Reference 3.

The association between aircraft hazard and radar echo intensity distribution is considered in more detail in Section 2.0. The use of radar in the detection of the small convective cells within a radar echo contour is considered in Section 3.0. Cell tracking and forecast feasibility is considered in Section 4.0. The radar system requirements for cell detection are considered in Section 5.0. Conclusions and recommendations are presented in Section 6.0.

Table I	
REQUIRED RADAR SYSTEM CHARACTERISTICS	
Range Resolution	< 1 km (0.5 nmi)
Transverse Resolution (range x beamwidth)	< 3 km (1.6 nmi)
Precision	0.5 dB
Accuracy	5 dB
Peak Cell Intensity Detection Range	30 - 65 dBz
Update Rate	2 - 3 min
Polarization	Linear or orthogonal circular

2.0 HAZARD DETECTION HYPOTHESIS

2.1 Convective Turbulence

The remote detection of hazardous regions within thunderstorms using radar requires proper interpretation of the data to deduce regions of potential hazard. The Thunderstorm Project Report [4] suggested that the hazardous regions are collocated with regions of increased reflectivity. Burnham and Lee [5] and Lee [6] have considered the association between turbulence and reflectivity and found that the simple pairing of regions with high reflectivity and convective turbulence did not work, Lee [6] reported finding regions with turbulence and low but measurable reflectivity and regions with high reflectivity and no turbulence. He suggested the use of Doppler radar because of the apparent lack of correlation between turbulence and reflectivity. Although Doppler radars have the potential of detecting the hazardous regions, direct detection of turbulence at the spatial scale responsible for aircraft hazard is not practical (see Appendix). Unfortunately, indirect techniques which may prove practical have not been developed as yet. One potentially attractive indirect technique is to exploit the spatial variation in mean velocity.

A physical model for the generation of turbulence within a thunderstorm suggests that small local increases in reflectivity should occur in the vicinity of the thunderstorm updrafts. Aircraft observations have shown that turbulence occurs primarily in the updraft regions [7]. A schematic view of the updraft and downdraft currents within a thunderstorm cell is given in Fig. 1 (see [8,9]). Observations of turbulence within thunderstorms reported by Chernikov et al [10] show turbulence within the updraft regions at a number of different heights within a cell. Heat energy released by the condensation of water vapor carried aloft in the updrafts drives the currents shown on Fig. 1. The moisture carried aloft condenses to form cloud particles which grow within the updraft region to form larger particles that are detectable by radar [8]. The cloud particles and larger precipitation particles which are initially formed in the updraft region are transported to other regions within the cloud system by the updraft and downdraft currents. The precipitation particles grow and fall relative to the air in which they are imbedded. Downdrafts are created both by evaporative cooling and by the drag of the falling particles. The updraft regions

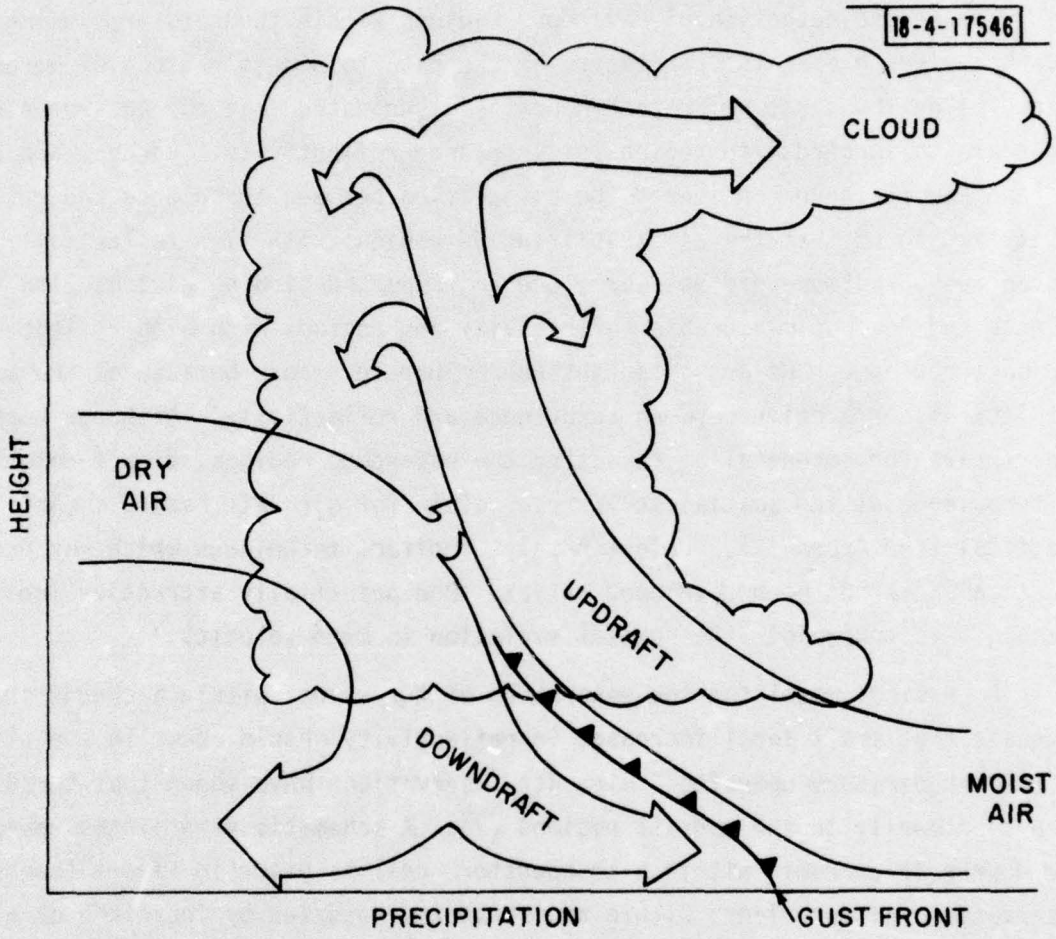

Fig. 1. Updraft and downdraft structure within a convective cell.

should be detectable by radar as regions with small relative increases in reflectivity (liquid water content). The relative increases are caused by the updraft moisture source; the lower level reflectivity regions surrounding the local maxima correspond to the regions through which the liquid water is dispersed after being generated in the updraft.

2.2 Detection Hypothesis

The updraft regions produce both convective turbulence and local increases in radar reflectivity. The local reflectivity increases can be detected on reflectivity maps as indicated on Fig. 2. Relative maxima are located at 1 and 2 on the contour plot. Two distinct cells are declared when the valley between the peaks is lower than the threshold value, T, measured from the lower peak. The areas within contours T decibels below each peak are the cells. Cells are declared only for contours that enclose no other cells.

Updrafts produce only small relative increases in reflectivity. The threshold value must be small enough to detect all the updraft regions but large enough to be unaffected by the statistical noise of a reflectivity map. Observations of cells within a thunderstorm region obtained with the high precision Millstone radar [11] are depicted on Fig. 3. These data show a number of cells using a 2.5 dB value for T. As the value for T changes, the number of cell detections changes. Using T = 2.5 db, 11 cells were detected; T = 5 dB, 8 cells were detected, and T = 10 dB, 5 cells were detected. Since the apparent number of cells depends upon the threshold, the question to be asked is which is the correct number. In this case, it is expected that the number of cells (updraft regions) is 11 or more. Areas that exist as broad shoulders on lower level contours may also contain cells. Such an area is evident to the northeast of the furthest north 42.5 dB peak reflectivity cell. This area may contain a cell that was not detected because the threshold value was too large.

The threshold value cannot be made arbitrarily small. Radar measurements are statistical in nature and an observed reflectivity value is only an estimate of the true value [12]. The measurement error (precision) associated with

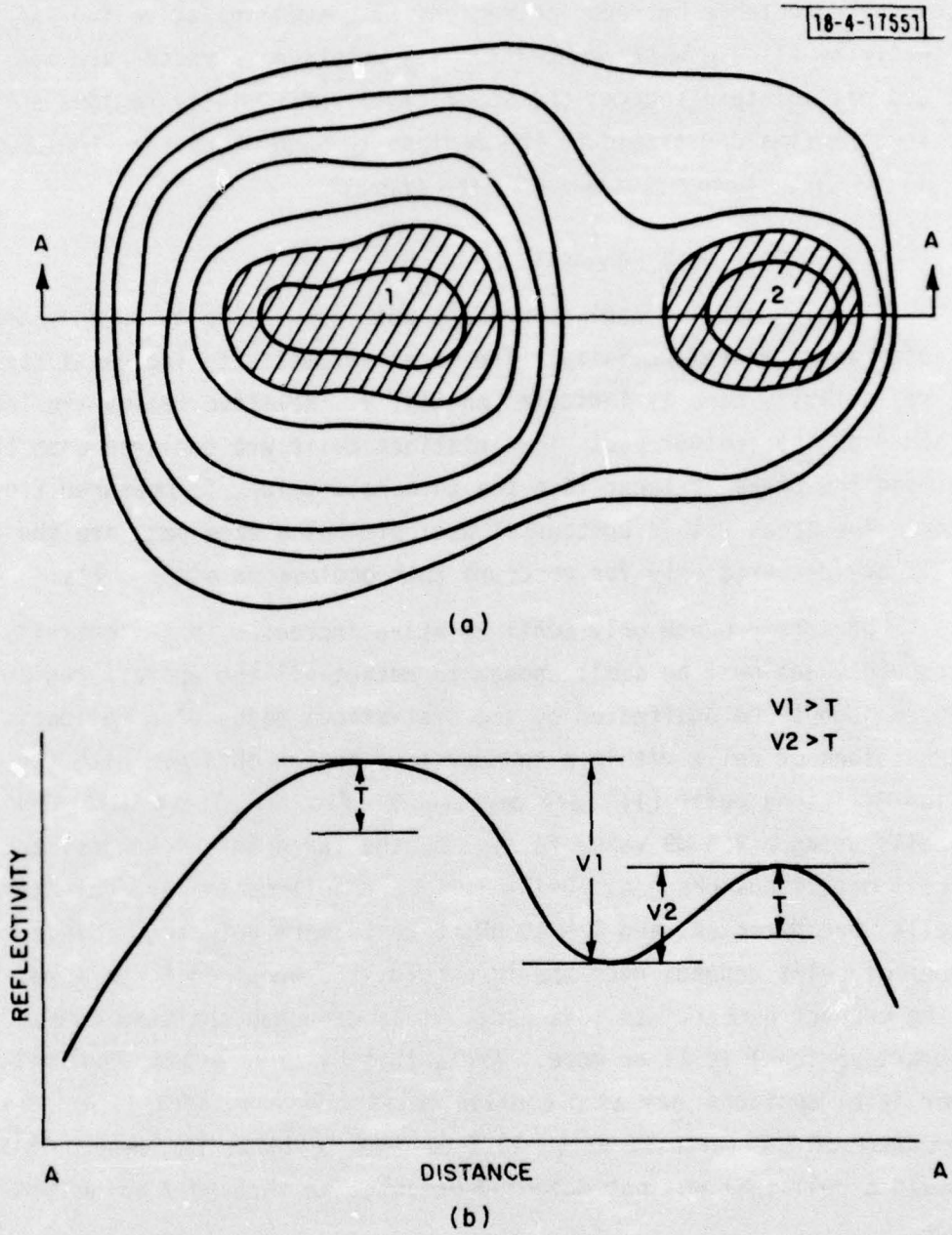

Fig. 2. Schematic illustration of the cell detection algorithm.

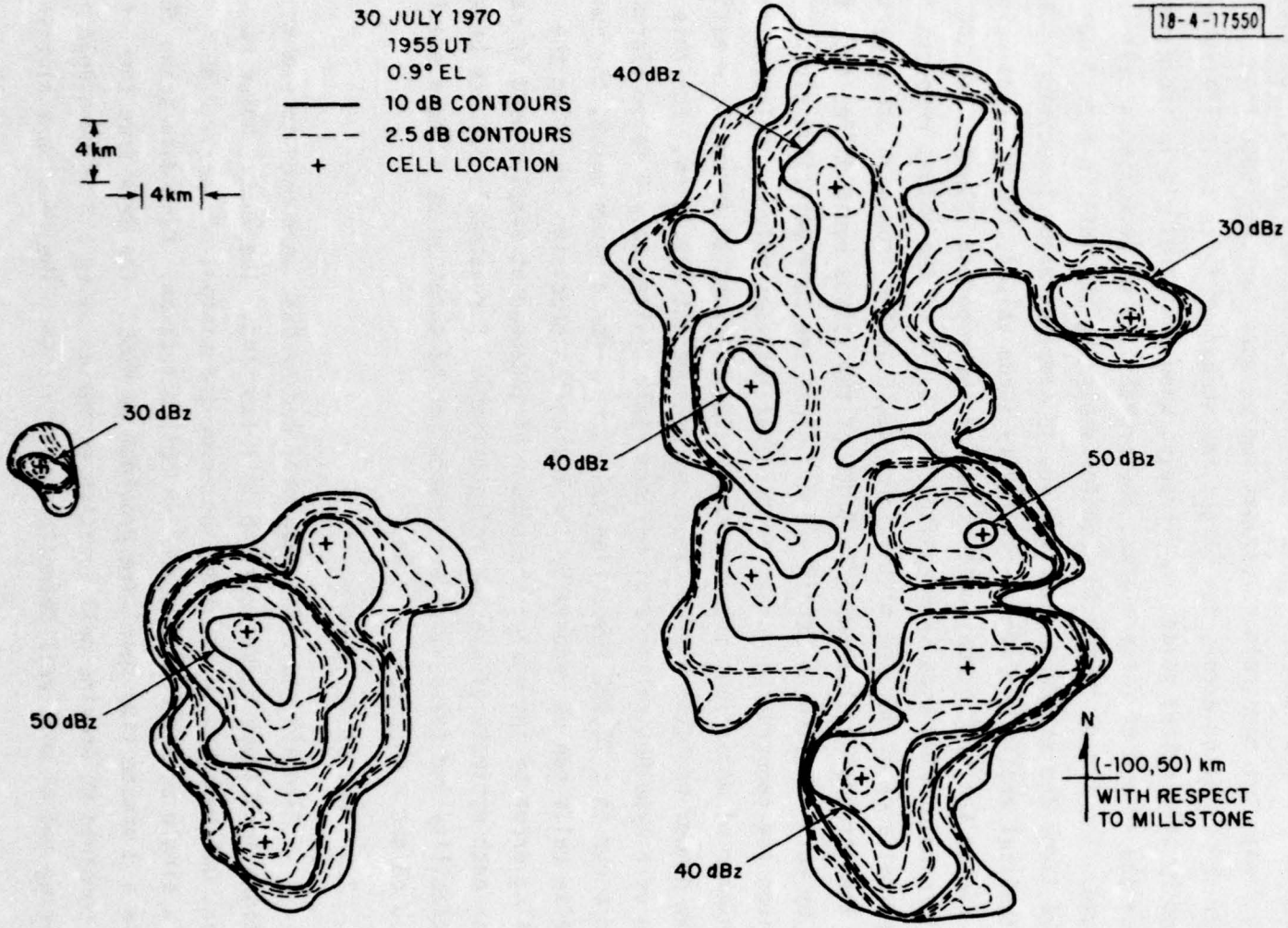

Fig. 3. Radar reflectivity contours and cells detected using a 2.5 dB threshold.

the use of a fixed number of samples to estimate the average reflectivity value limits the threshold value that can be used for cell detection. The larger the sampling error, the larger the number of false cells (false alarms) caused by statistical noise. Conversely, when the threshold is increased to reduce the number of false alarms, the probability of detecting a cell is decreased. The 2.5 dB threshold used for analyzing the data in Fig. 3 was roughly 3.6 times the standard deviation due to sampling error (precision). For a hypothetical area of uniform reflectivity (true value), the apparent values will vary due to the statistical uncertainty of the reported values. For the precision and threshold value used in preparing Fig. 3, 1% of the values reported for a hypothetical area of uniform reflectivity would differ from each other by more than the threshold value and only 0.02% of the values would differ from the mean by more than the threshold value. Since the cell detection algorithm requires the construction of a contour that includes only one relative maxima, the number of deviations from the mean value provides an approximate estimate of the number of false alarms caused by measurement precision. For this example of a hypothetical area of uniform reflectivity, only 2 false alarms would occur in a 10,000 resolution cell area. For a given value, the number of false cells can be reduced by increasing the precision (reducing the sampling error by increasing the number of independent samples used in calculating each estimate of average reflectivity). A reasonable balance between detectability and false alarm occurrence can be obtained by using a precision of 0.5 dB and a threshold of 3 dB.

2.3 Test of Hypothesis

Aircraft and radar data provided by NSSL were used to examine the relationship between turbulence and cell location. The NSSL Doppler radar at Norman, Oklahoma had an rms sampling error (precision) of nearly 2 dB. Data from a single scan were not useful in cell detection. Nine data scans obtained within a 3 minute time span were provided by NSSL. The data from these scans were combined to provide cell location estimates using a 3 dB threshold and requiring two or more cell detections within 1 km. The resultant plot showing

cell locations (radar measurements) and turbulent regions (aircraft measurements) is shown on Fig. 4. The locations of regions within the 40 dBz contours on at least one scan (dashed) and all scans (solid) are also shown on the figure. The large separations between the dashed and solid curves are evidence of contour position uncertainty caused by sampling errors. Cell to track associations with less than 3 km (1.6 nmi) separations are indicated on the figure by dot-dashed lines.

The data show a good correlation between turbulent regions and cells. The strongest region of turbulence is within 3 km of a cell that has peak reflectivity values that range from 57 to 59 dBz depending upon the scan. Six regions of light turbulence are displayed, four of which are within 3 km of cells. One cell was detected that was within 3 km of the track but did not produce noticeable turbulence. Based upon this single aircraft track and rather imprecise radar data, excellent agreement was obtained and the cell-turbulence association hypothesis appears to be correct.

The data displayed in Fig. 4 (and Fig. A2 of the appendix) are for a single aircraft penetration of a single storm and do not constitute a statistical test of the hypothesis. The hypothesis was advanced on physical grounds and supported by other measurements as noted in section 2.1 and in the appendix. The comparison shown on Fig. 4 is presented only to show that the hypothesis is reasonable and not contradicted by the sample of data provided by NSSL. To fully test the hypothesis, a number of comparisons should be made. A larger sample of data is available at NSSL which could possibly serve this purpose.

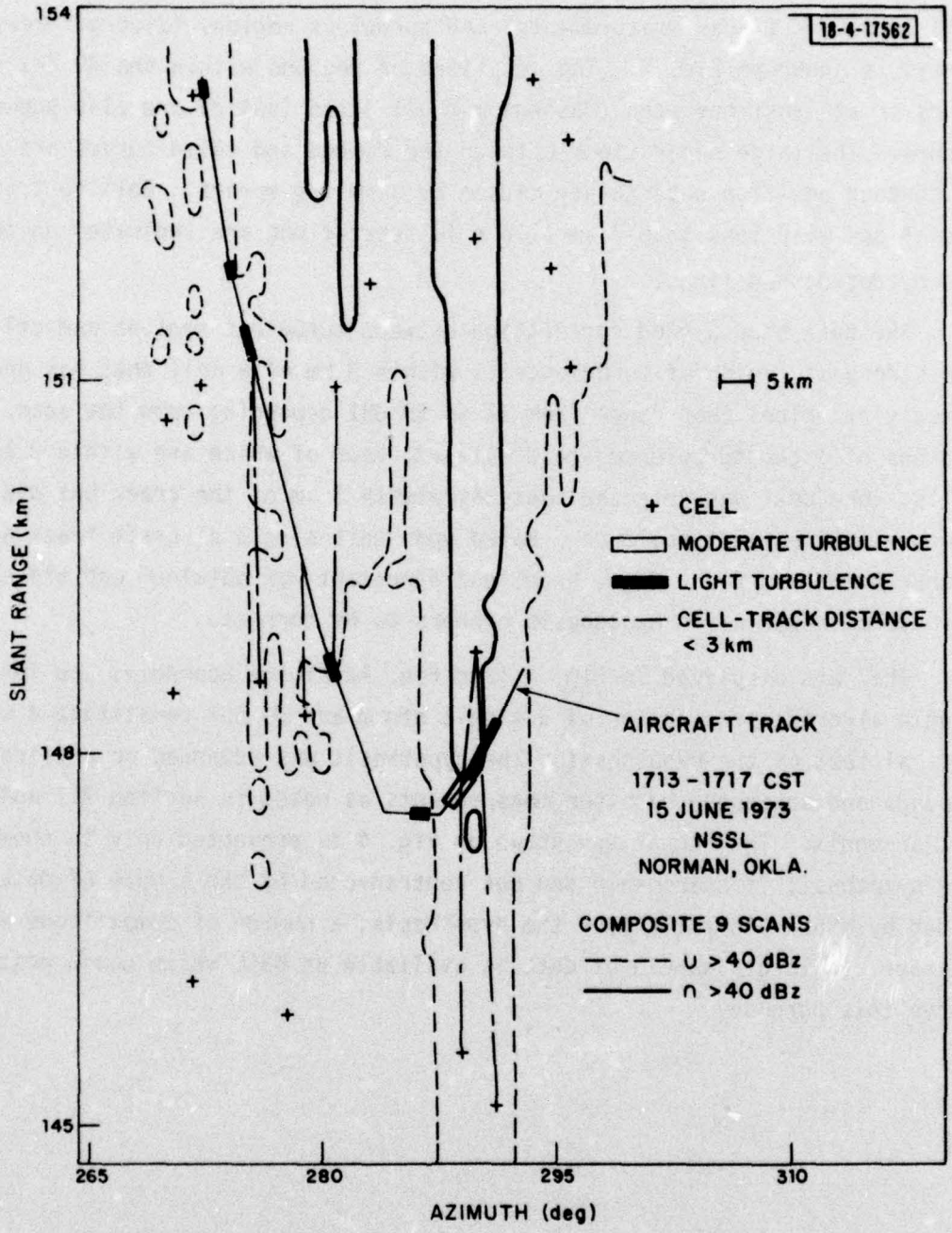

Fig. 4. Detected cells and aircraft turbulence in a thunderstorm.

3.0 CELL DETECTION

3.1 Reflectivity Structure

The hazard detection hypothesis was used to locate cells in a large sample of data obtained in coastal Virginia. The detection algorithm found a number of cells both within high reflectivity regions and in surrounding regions of lower reflectivity. For an operational system it is recommended that only the cell locations be displayed. (see section 3.0 of reference 1)

The weather radar data displayed in Figs. 5-7 were obtained at Wallops Island, VA, by the Johns Hopkins University Applied Physics Laboratory (APL) for the National Aeronautics and Space Administration.* The SPANDAR S-band radar was used to obtain the data. The radar system as operated had a 0.4° beamwidth, 150 m pulse resolution distance, 0.5 dB rms measurement error (precision), and a 2 dB measurement accuracy [14]. The data were processed at MIT Lincoln Laboratory to form radar reflectivity maps on a rectangular grid with a linear spatial resolution of 1 km (0.5 nmi). The reflectivity maps were further processed by computer to : (1) provide reflectivity contour maps, (2) to detect cells using the algorithm discussed above with a 3 dB threshold, (3) to combine cell detections to provide detection probability estimates, and (4) to track the cells.

The SPANDAR data were obtained between 2000 and 0400 UT (1600-2400 local time) on days with rain in the Wallops Island area during the summer of 1973. Data obtained between 13 June and 10 July were used to analyze the performance of the cell detection algorithm. The data were gathered using azimuth-elevation raster scan sequences (tilt sequences). A limited azimuth sector was scanned using a series of azimuth scans at elevation angles selected to observe a storm at a number of heights. A raster scan sequence typically took between 3 and 5 minutes to complete and was repeated at random time intervals. Series of raster scans with less than 10 minutes between raster scan start times were selected for analysis and to study cell tracks.

*Data provided by Dr. J. Eckerman, NASA Goddard Space Flight Center.

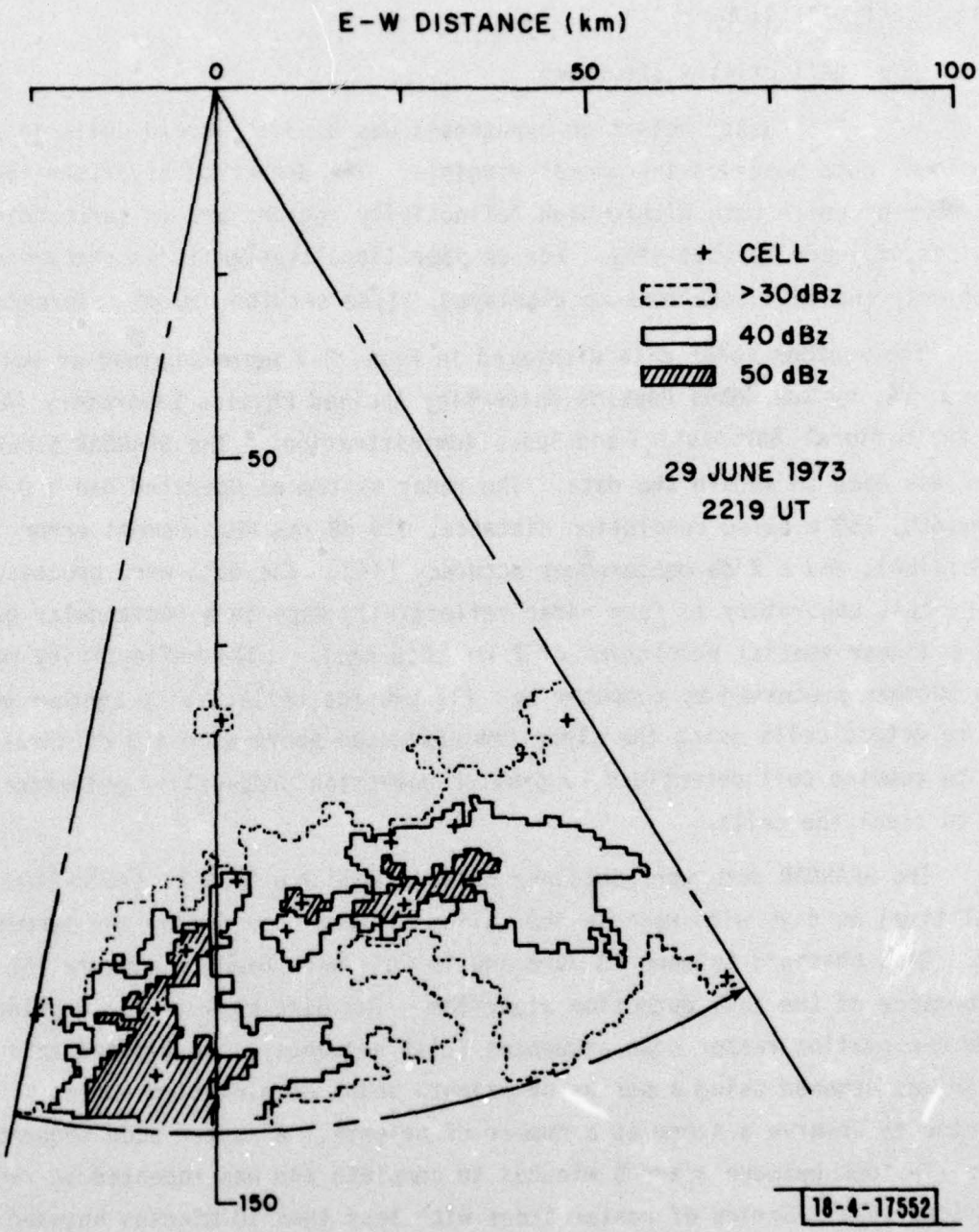

Fig. 5. 10 dB contours and cell locations 2219 UT, 29 June 1973.

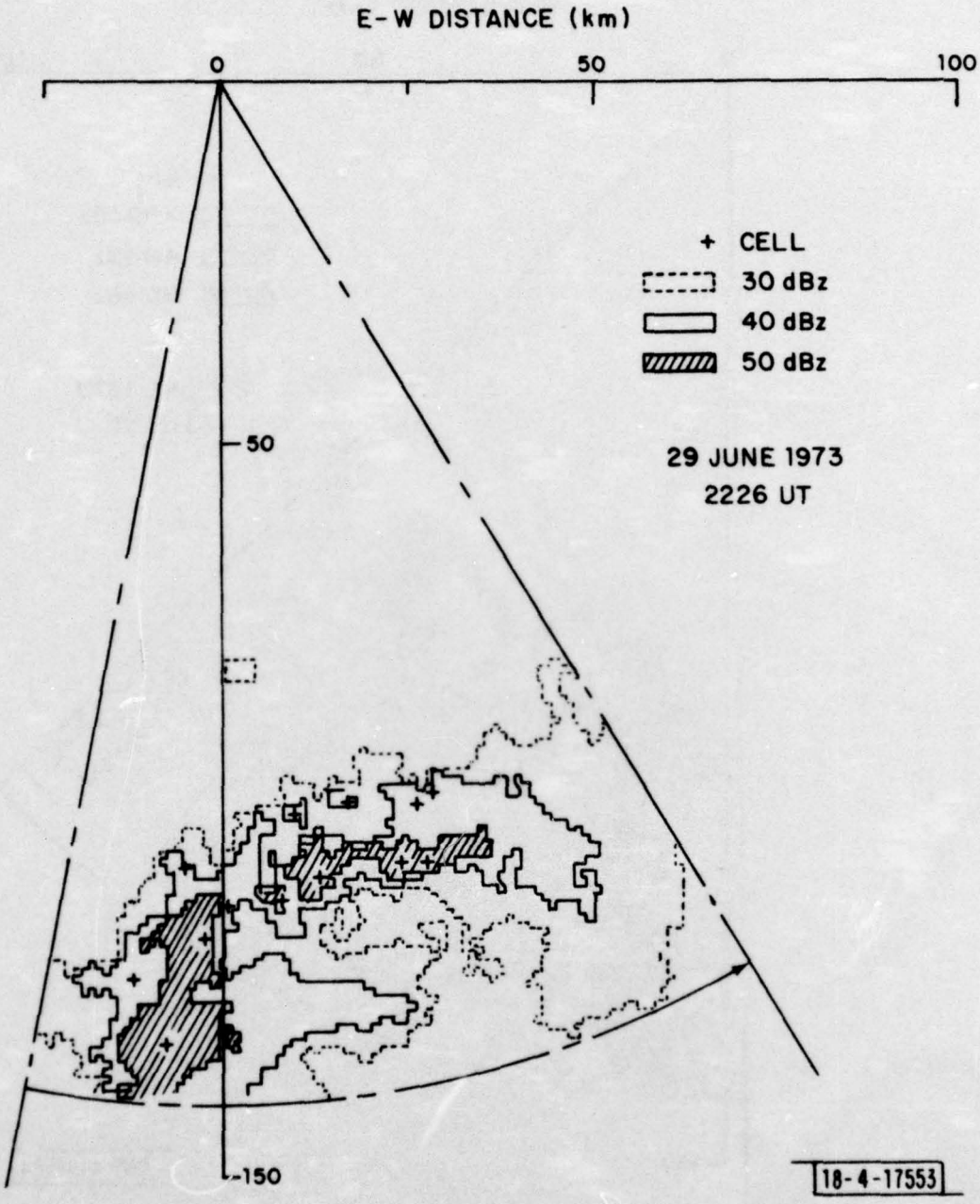

Fig. 6. 10 dB contours and cell locations 2226 UT, 29 June 1973.

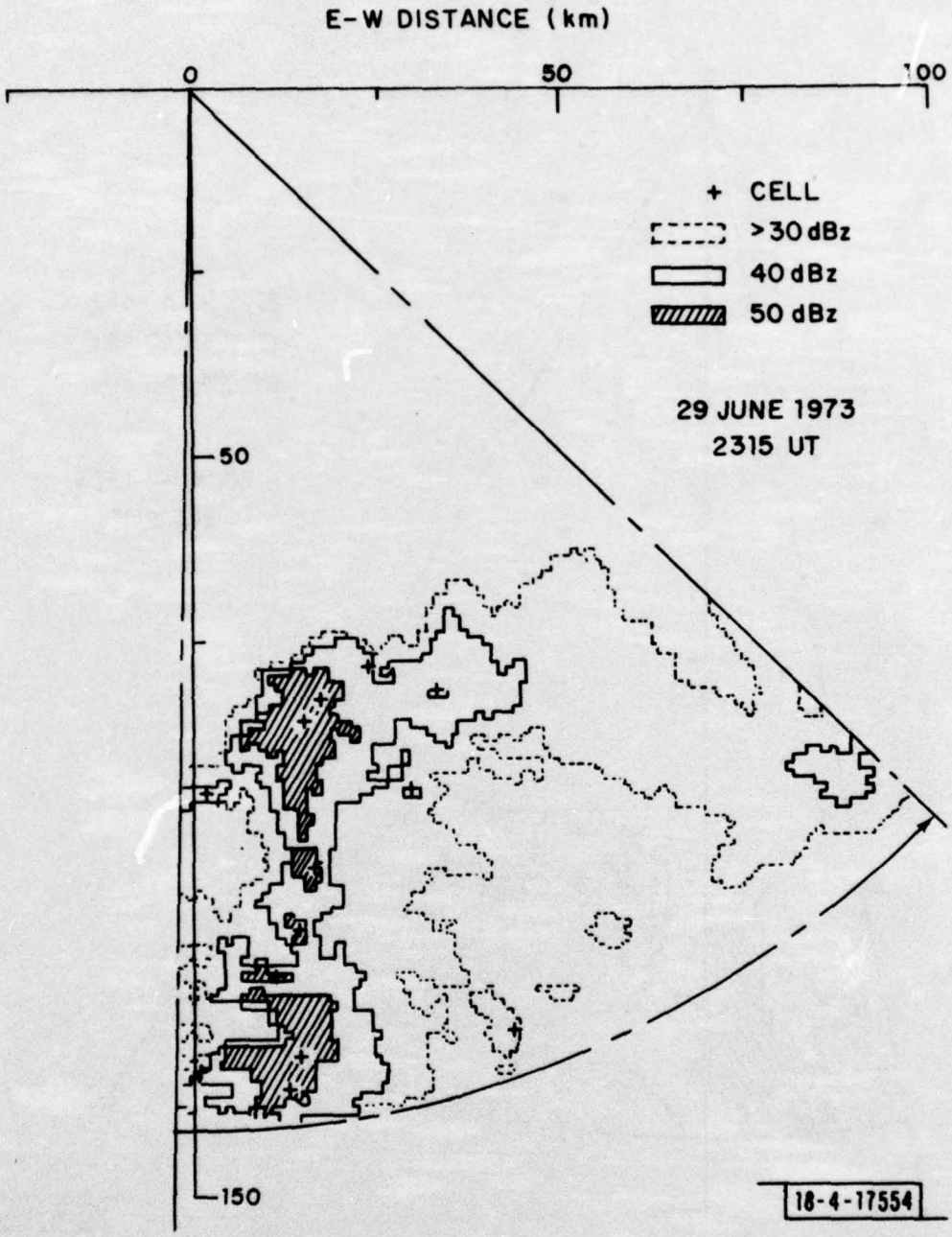

Fig. 7. 10 dB contours and cell locations 2315 UT, 29 June 1973.

The cell detection program was run for each azimuth scan of a raster scan sequence. The data obtained at heights of less than 6 km were combined to provide a best estimate of the cells in the scan area. Data obtained at heights below 3 km were used to obtain cell detection statistics.

Figures 5 through 7 show contour maps obtained at the lowest elevation angle of each raster scan and the best estimates of cell locations obtained from several azimuth scans within a raster scan. These data show a number of cells both within the highest reflectivity contours and in the areas surrounding the highest reflectivity contours.

3.2 Detection Statistics

The Wallops Island data were processed using a 3 dB threshold (see Fig. 2 for threshold definition). Preliminary analysis of data using a 5 dB threshold resulted in reduced single scan detection probabilities relative to the 0.6 to 0.9 values obtained for the 3 dB threshold. Detection probabilities were obtained using cells independently detected on each azimuth scan of a raster scan sequence. Starting with the lowest elevation angle the locations of cells observed at higher elevation angles were compared with lower elevation angle cell locations. Cell detections at different heights were attributed to the same cell if the horizontal locations of the centers of mass of the cells were separated by less than the square root of the average of their areas. Cell detections were also combined if separated by less than the distance a cell could move between observations with a translation velocity of 30 m/s (60 kts). In applying the cell association criteria, an additional position uncertainty of 1 km for each cell was included to account for possible errors in computing cell location. If more than one cell on a particular scan met the criteria for association with a cell on another scan, the pair with the smallest separation distance was used. After the cell associations were made, cell detection statistics were generated.

A detected cell that was not associated with any other detected cells at other heights was classified as a possible detection (P-cell - a possible cell classification used as an aid in generating detection statistics).

Generally more than 4 observations were possible at heights below 6 km (20 kft); hence a P-cell could represent a cell with a probability of detection less than 0.25 or it could be a false alarm. A maximum height of 6 km was used in locating cells because the reflectivity values were generally weaker and the reflectivity structure was often more complex above that height. The best estimate location, intensity, and area of each cell was determined by averaging observations made at heights below 3 km (10 kft). A 3 km height was used for this operation because observations reported by Crane [15] in Virginia showed that the reflectivity structure changed little in summer convective storms at heights below the freezing level. The freezing levels for the Wallops Island data set were generally at heights above 4 km. The height of each cell was determined by locating the altitude at which the average reflectivity value decreased 5 dB below the largest average value for the cell.

Cell and P-cell locations for each raster scan sequence in a series of 5 raster scans are displayed on Fig. 8. The P-cells identified as ground clutter were obtained only at the lowest elevation angle and did not move. Two cells were observed to last the entire time period. Both had an average velocity of 9.4 m/s (18 knots) and reasonably constant peak reflectivity values. Some of the cells tracked in Fig. 8 were always or partially listed as P-cells. These were weak with peak values less than 42 dBz. In these cases, P-cells represent cells with low detection probabilities. Only one P-cell detection was a false alarm that could not be identified either as a weak cell or as ground clutter and presumably was an aircraft. The actual cells displayed on Fig. 8 (cells and P-cells that moved) are entities that can be identified and tracked for periods of time ranging from 6 minutes for the weakest cell (track 4) to 48 minutes for the more intense cells (tracks 2 and 7).

Detection probabilities were generated for each cell that remained after the association test. The detection probabilities were obtained by determining the ratio of the number of cell detections made at heights below 3 km (10 kft) to the number of opportunities for cell detection at heights less than 3 km.* Cell detection histograms were generated using 5 dB

*The cell population is assumed to be the cells detected at more than one altitude below 6 km. The number of opportunities is the number of azimuth scans in a raster scan for which these cells should be seen below 3 km. This is range dependent.

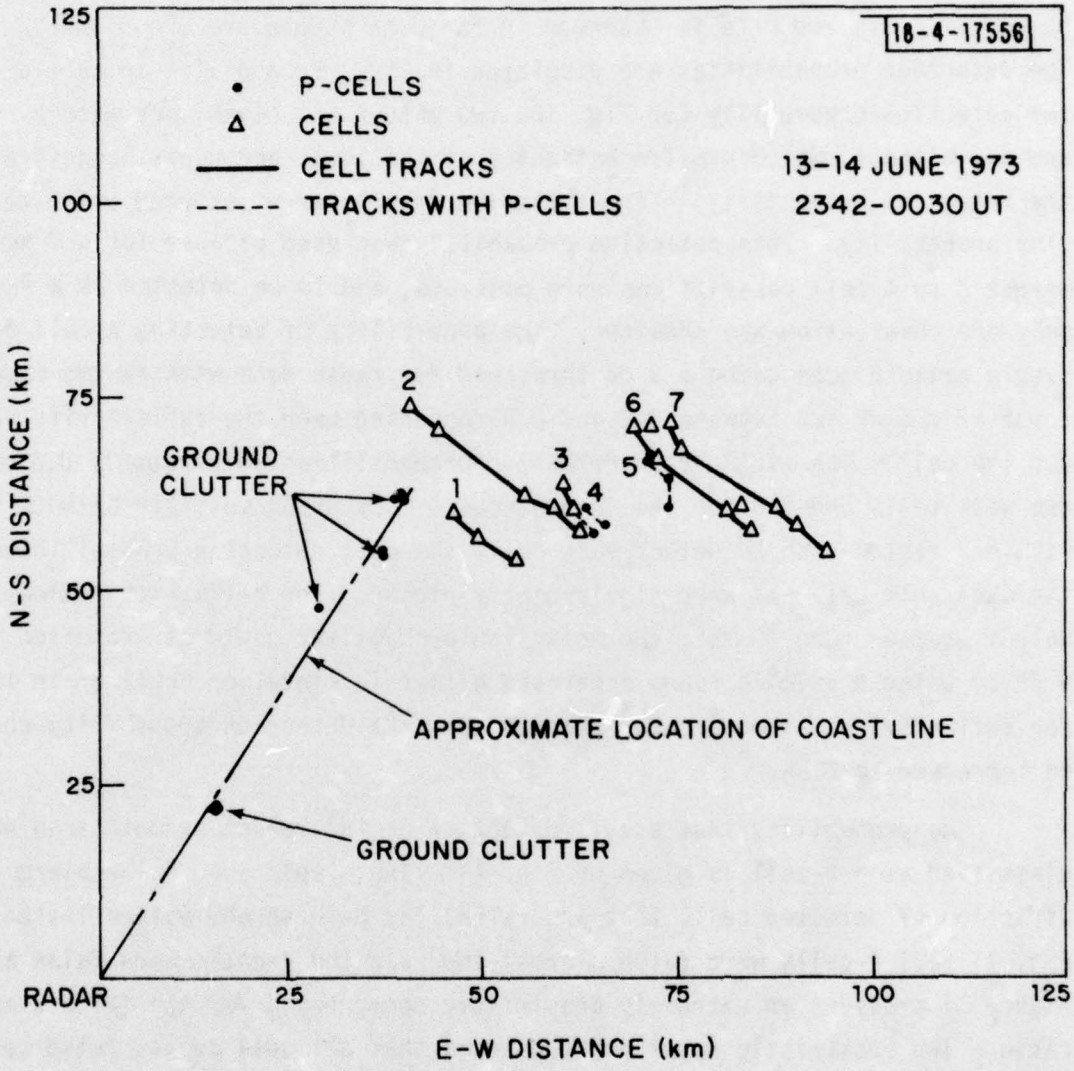

Fig. 8. Cell tracks, 14 June 1973.

reflectivity and a 5 km^2 area sorting bins. Summaries of detection probabilities and P-cell occurrences were constructed for the June-July data set. The total number of cells and P-cells observed in the data sample are shown in Fig. 9. The detection probabilities are displayed in Figs. 10 and 11. In tabulating the detection probability for Fig. 10, two values are given, one with P-cells and one without, which provide estimates of the lower and upper bounds for the detection probability.* For inclusion P-cells were assigned a 0.3 detection probability. This detection probability was used because for a 3 km height 3 to 4 cell observations were possible, and to be detected as a P-cell only one observation was obtained. The probability of detecting a cell on a single azimuth scan using a 3 dB threshold for radar data with an rms sampling error of 0.5 dB was between 0.5 and 0.9 depending upon the reflectivity value for the cell. The single scan detection probabilities were roughly 0.6 for the weak cells and 0.8 for the intense cells. By using multiple azimuth scans within a raster scan to detect each cell, the cell detection probabilities for the June-July data set were significantly higher. For cells with reflectivity values greater than 45 dBz, the detection probability could be increased to 0.98 by using 3 azimuth scans separated either in elevation angle or in time. For reflectivity values greater than 35 dBz, the detection probability could be increased to 0.94.

The probability that a cell detection on the lowest azimuth scan was classified as a P-cell is given on Fig. 11. The single scan false alarm ratio (fraction of detected cells that are false) lay between the values listed on Fig. 11 (all P-cells were false alarms) and zero (no P-cells were false alarms). Figure 11 provides an extremely pessimistic upper bound for the false alarm ratio. The pessimistic upper bound assumes that all weak cells, false cells, aircraft and ground clutter occurrences were false alarms. Observations, when track data were available, showed that most P-cells were either weak cells or ground clutter. The false alarm ratio therefore is quite low, less than 0.03 on a single scan and may be significantly lower than this if aircraft can be independently identified.

*The concept of P-cells was introduced to permit this bound and a corresponding one for false alarm probability. This was required since there was no independent measurement of the true cell population which thus had to be bounded from the radar data.

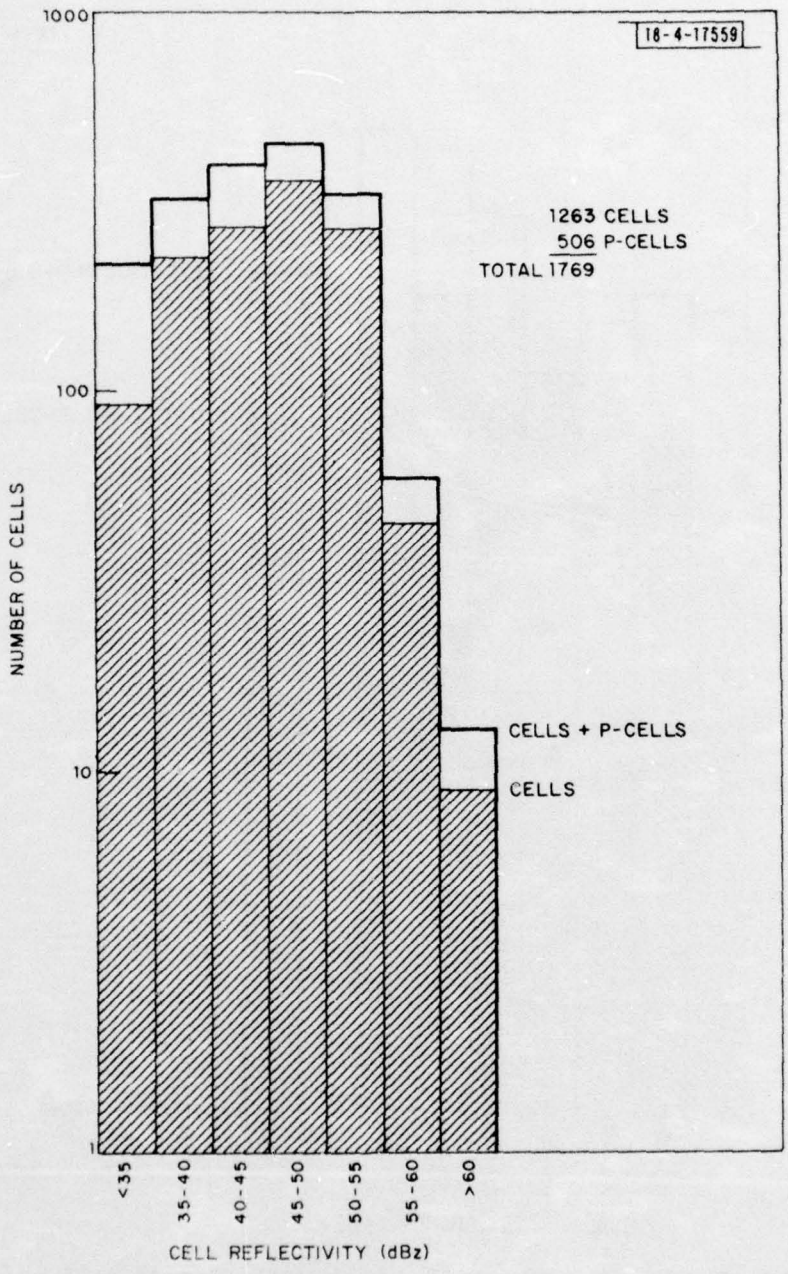

Fig. 9. Number of cells observed vs peak cell reflectivity.

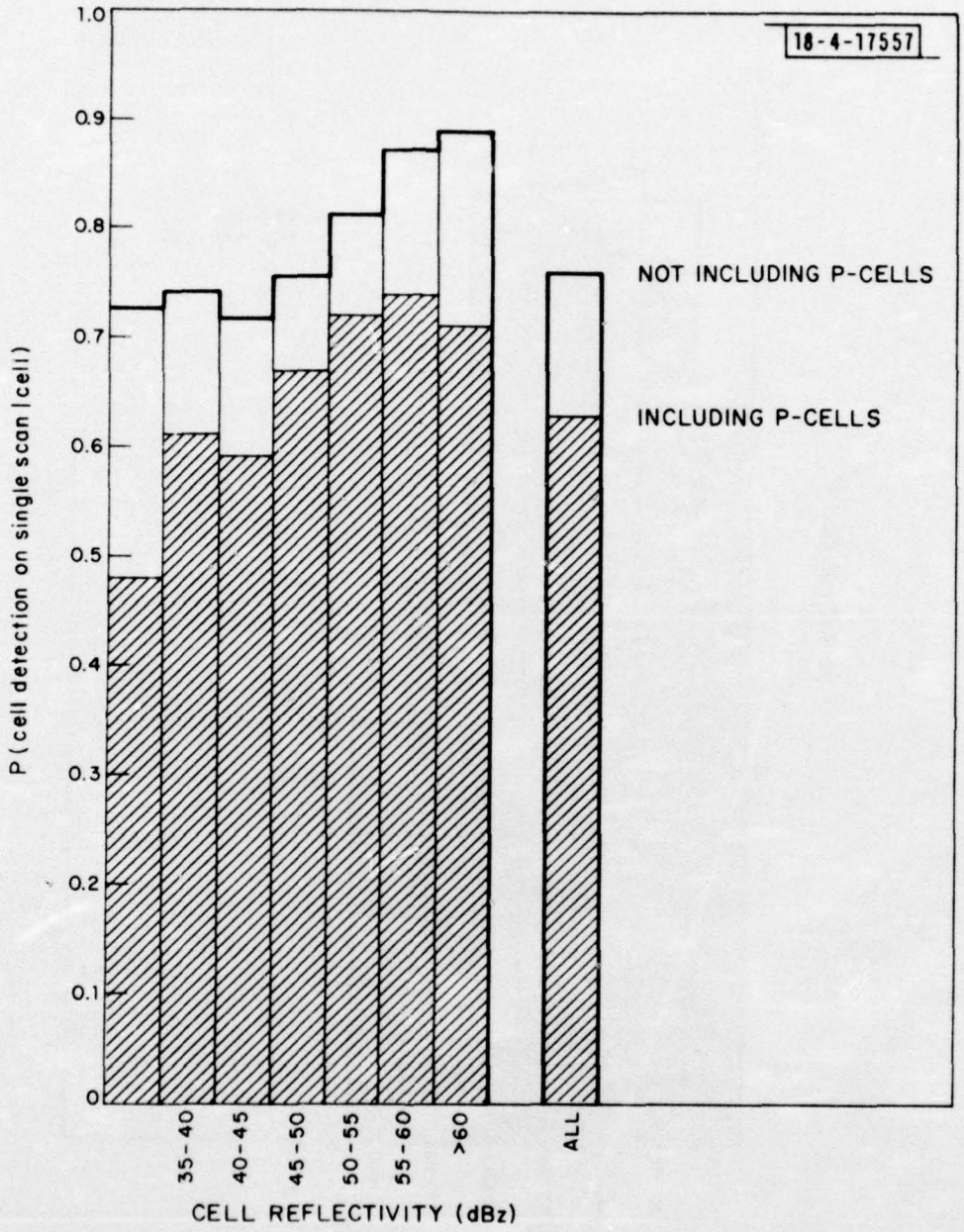

Fig. 10. Single scan detection probability vs peak cell reflectivity.

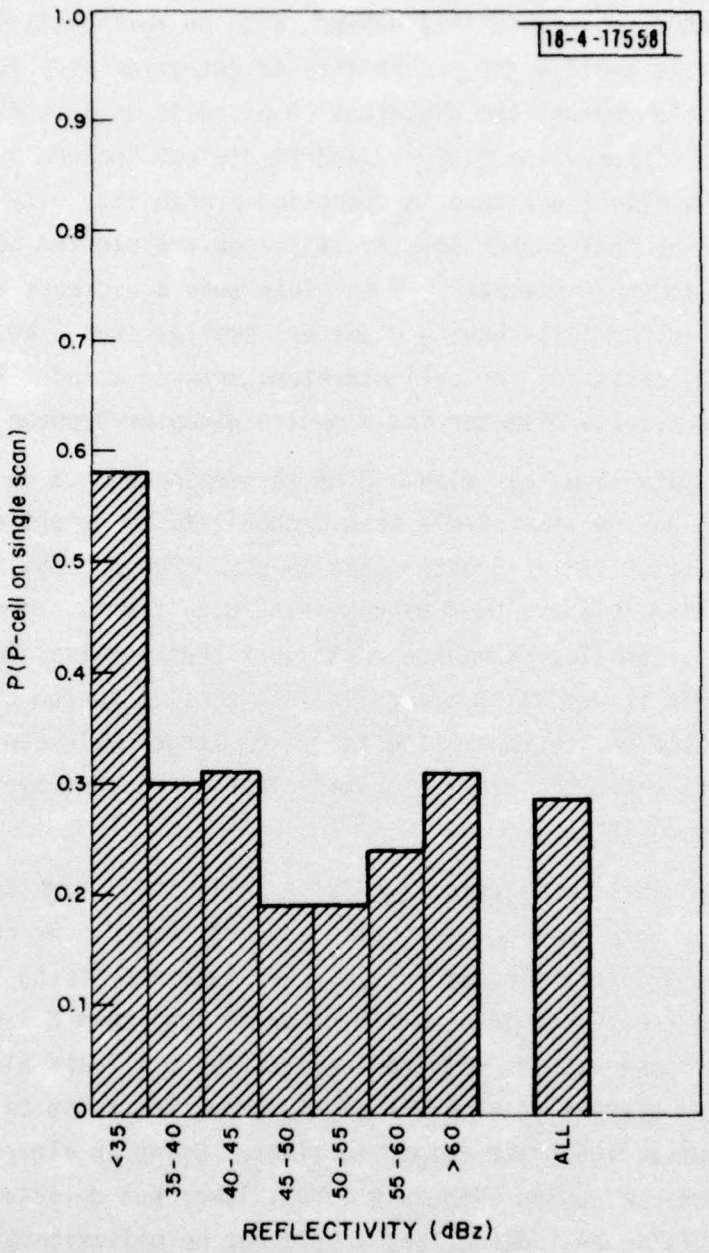

Fig. 11. Single scan P-cell detection probability vs reported reflectivity.

The detection probability depends both on reflectivity value and cell area. Figure 12 depicts the probability of detection as a function of cell area and Fig. 13 depicts the distribution of cells as a function of cell area. The data used in compiling Figs. 12 and 13 did not include P-cells. These figures show a slight decrease in detection probability with increasing cell area. Empirical cell number density estimates are plotted both as a function of cell area and cell diameter. Both plots show a decrease relative to the exponential fit for cells having diameters smaller than 2 km (1.1 nmi). The number density maximizes for cell diameters between 2 and 3 km. The cells have a 2.9 km average diameter and a median diameter between 2 and 3 km.

These data show that with a 3 dB threshold and 0.5 dB precision, the pessimistic bound for the single scan probability of detection exceeds 0.6 for cells with reflectivities greater than 35 dBz. The probability of detection can be increased to above 0.94 by combining data from 3 or more azimuth scans. The cell detection algorithm appears to work best for isolated cells and degrades mainly in detecting all cells in a closely spaced group. Small cells with too small a valley separating them from large cells can be missed. However, aircraft would be advised to stay clear of these groups and thus also avoid the missed cells.

The probability of detecting false cells is unacceptably high unless ground clutter returns can be detected and suppressed. By removing ground clutter (see [3]) in the radar receiver and data processing, the false alarm ratio can be reduced to less than 0.03 or to less than 0.1 on 3 azimuth scans. For the radar observations reduced to date, the 0.1 false alarm ratio implies the continuous display of 2 to 3 randomly occurring false cells within the rain areas in complex widespread rain situations. Using an algorithm that keeps the cells within a region with rain (i.e., lower but detectable reflectivity values), the false cell detections should not be objectionable. If, in addition, aircraft echoes are identified and suppressed, the false cell detection problem should be reduced to only an occasional display of a false cell.

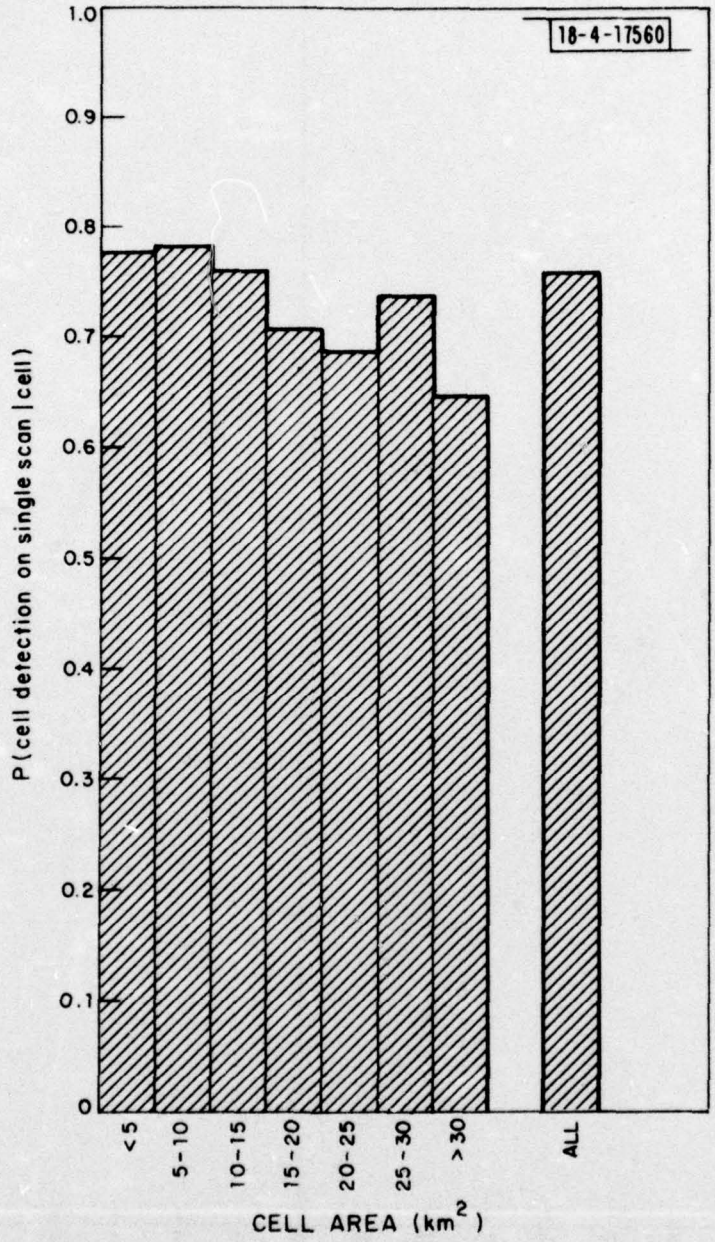

Fig. 12. Single scan detection probability vs cell area.

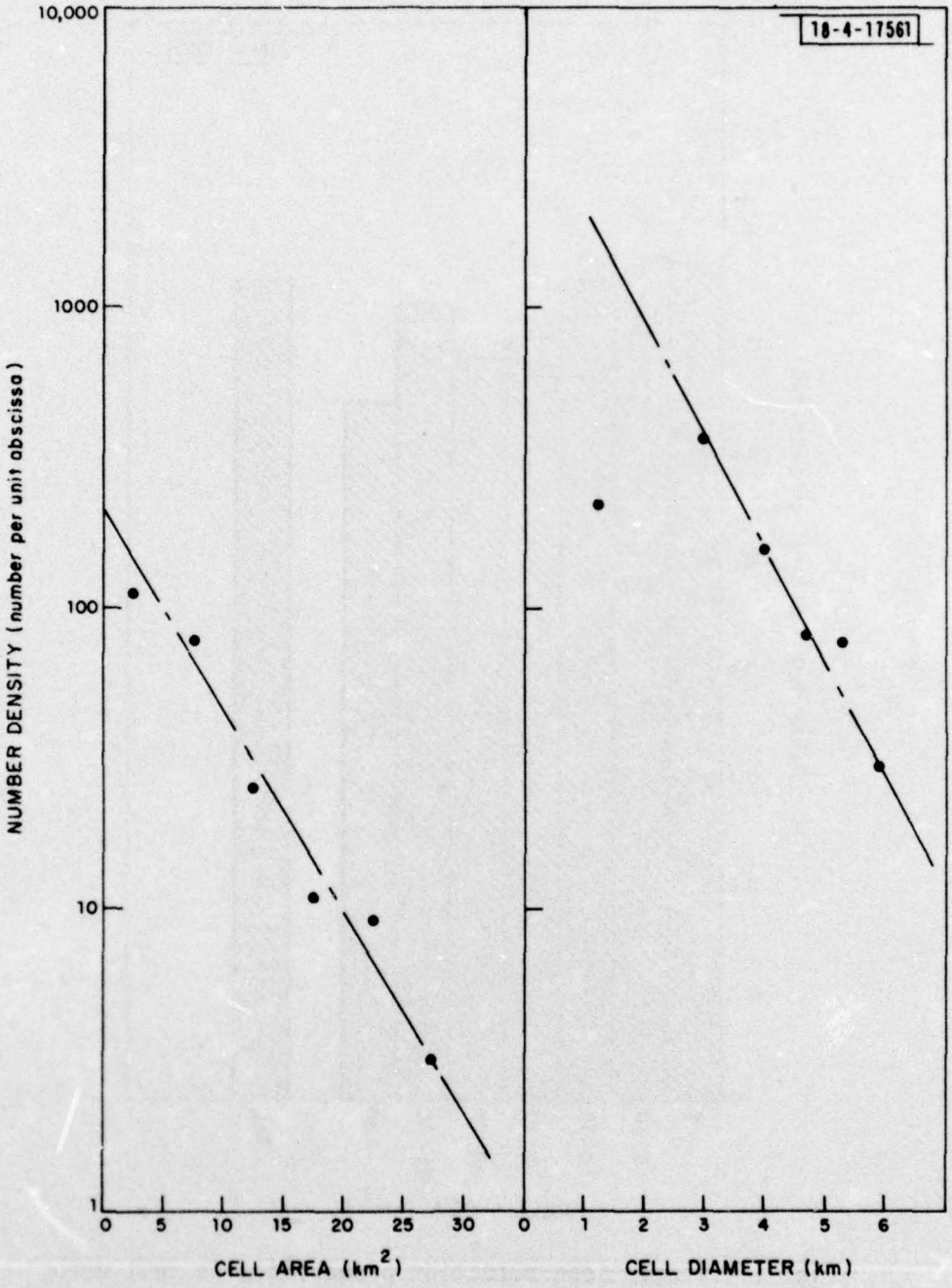

Fig. 13. Cell number density vs cell area and cell diameter.

These results show that the hazard detection algorithm is able to identify regions on the radar display that are potentially hazardous. The data on Fig. 8 show that these detected regions form tracks that move in a regular manner.

4.0 CELL TRACKING AND FORECASTING

4.1 Cell Tracks

One of the requirements of a viable hazard detection scheme is that it reliably finds hazardous regions. The second requirement is that the regions move in a regular manner that can be tracked. The cell detection statistics showed that the individual cells can be detected. Figure 8 showed that regular tracks were observed. Observations on other days show that tracks are always obtained. Analysis of data from one day show that the tracks have a 12 minute half life and that accurate cell position forecasts are possible for time periods up to 20 minutes. Although the average half life is smaller than the prediction interval, the more intense cells have longer lifetimes and thus the 20 minute forecast is useful for the more intense cells and presumably the more hazardous regions.

The echo areas and cells move with time. The fixed reflectivity contours translate and change shape as the individual cells within a contour grow, mature and decay. This process is evident in Figs. 5, 6 and 7. The observations depicted on Figs. 5 and 6 are separated by 7 minutes; the observations depicted on Figs. 6 and 7 are separated by 49 minutes. The contours displayed on Figs. 5 and 6 are similar in shape; the contours on Figs. 6 and 7 are not. 40 dBz contour plots for the data on Figs. 5 and 6 and data from observations made 7 minutes earlier are displayed on Fig. 14. Cell locations and cell tracks are also displayed on Fig. 14. The cells all move in roughly the same direction, the contours exhibit motion but different edges of the contours move at different rates.

The SPANDAR data set used for the analysis of the cell detection problem was of limited use in analyzing the tracking problem. The raster scans were taken at random time intervals generally with time spacings too large to allow cell association. Fortunately, two data sets were obtained during the summer of 1973 that were not raster scans but were a series of azimuth scans made at the same elevation angle with short time intervals between the scans. These data are shown in Figs. 15 and 16. The data on Fig. 15 are for 30 second intervals between observations. The data displayed on the figure are for all

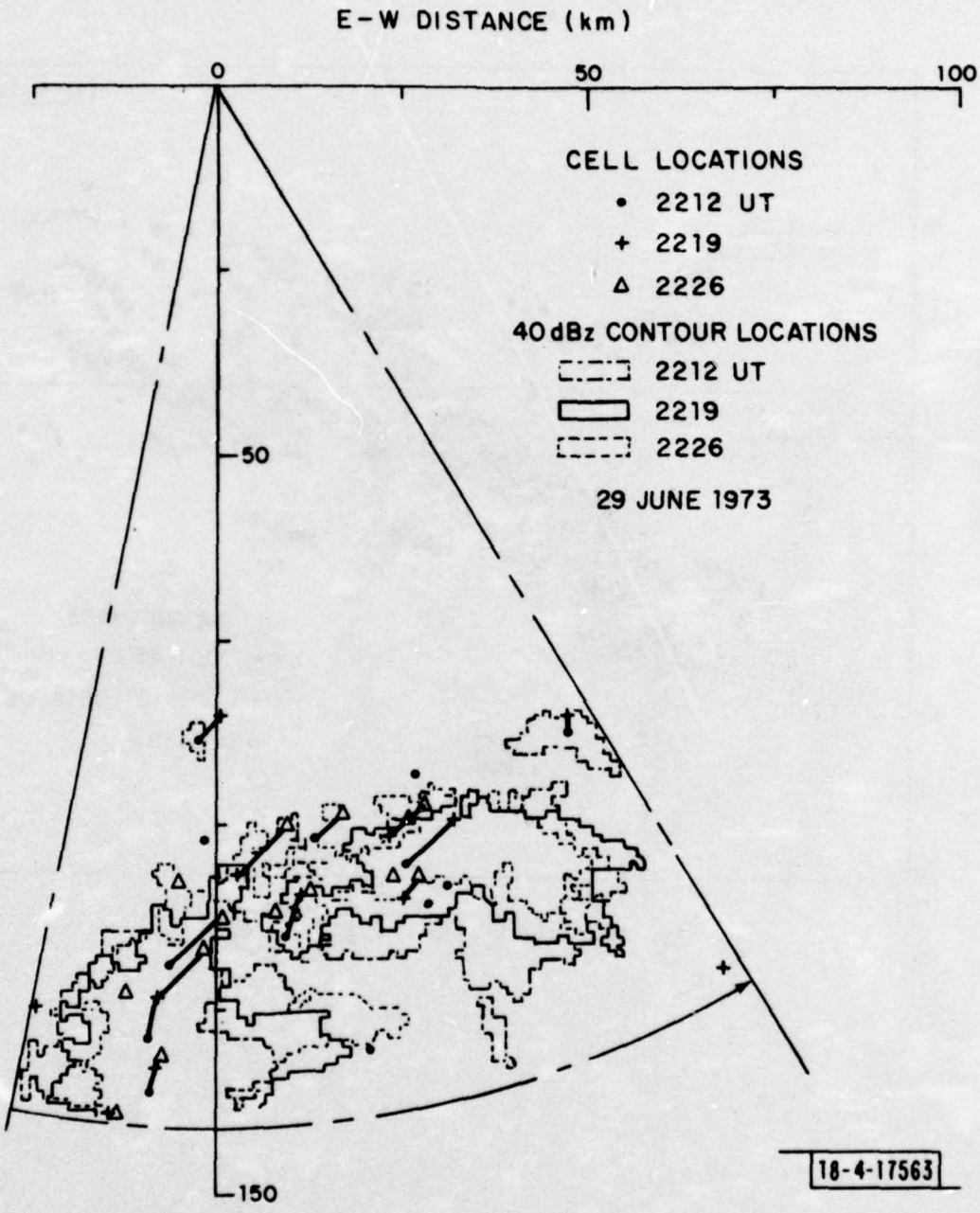

Fig. 14. Cell tracks, 29 June 1973.

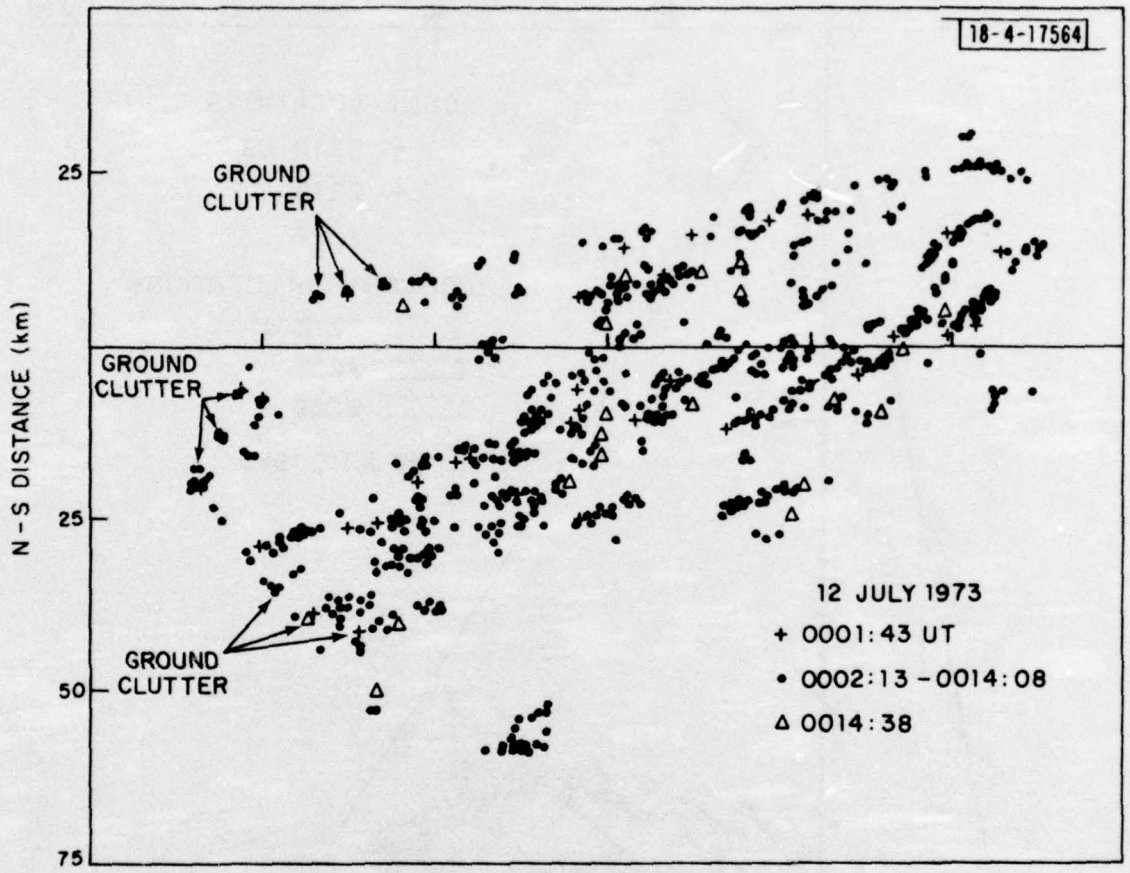

Fig. 15. Cell tracks, 12 July 1973.

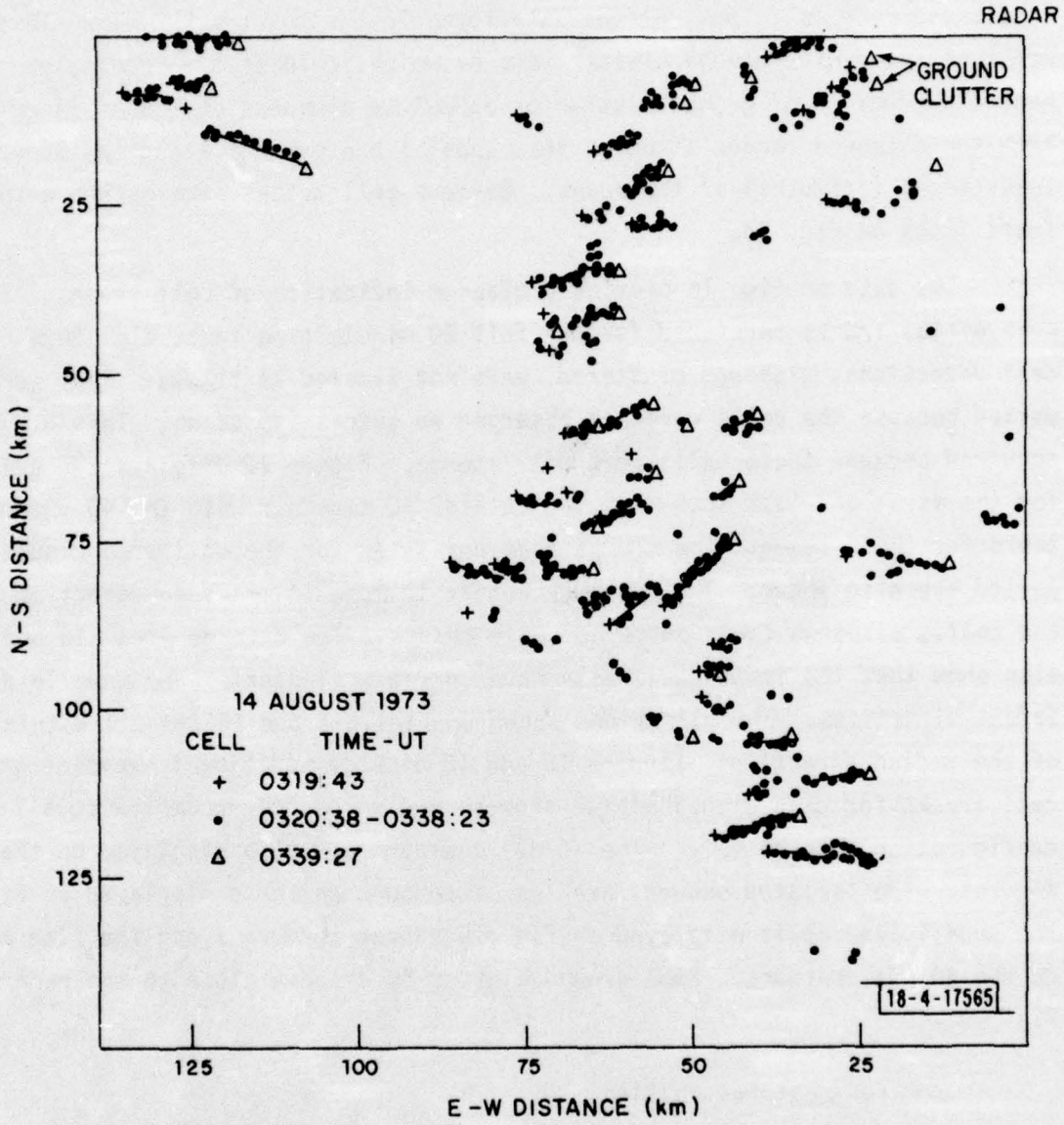

Fig. 16. Cell tracks, 14 August 1973.

cell detections: cells, ground clutter, weak cells, aircraft and false cells (cells and P-cells). Most of the data form clusters or tracks. The clusters are associated with ground clutter some of which is labeled accordingly. A number of regions of ground clutter or anomalous propagation echoes (judging from the extended ranges at which they appear) are evident along the upper and lower edges (azimuths) of the scans. Obvious cell tracks were marked with short lines on Fig. 16.

The data on Fig. 16 provide a clearer indication of cell tracks. Several of the tracks persisted for the full 20 minute time interval. Some of the cell detections, although clustered, were not labeled as tracks. They were not marked because the cells were not observed on successive scans. This perhaps occurred because these cells were not intense. Figure 17 displays the cells for the first and last scan depicted on Fig. 16 together with the 40 dBz contours for these scans. The tracks that persisted for the entire 20 minute period are also shown. The contours appear to move in the same direction as the cells, although their shape and size change. The data on Figs. 16 and 17 also show that the individual cells have curved trajectories and move in different directions. The directions shown on Figs. 15 and 16 are all within $\pm$ 45° of the median direction. Figures 18 and 19 display additional examples of cell tracks for days with isolated showers and with a more complex squall line configuration respectively. The 40 dBz contours are also displayed on these figures. The isolated showers are less intense than those displayed on Fig. 8. The squall line cells displayed on Fig. 19 appear to move along the line as do the 40 dBz contours. Some ground clutter is evident close to the radar on Fig. 19.

4.2 Forecast Feasibility

The examples of cell tracks were obtained under different synoptic conditions on different days. These examples show that the cells persist and can be tracked. The regular behavior of the tracks indicate that cell locations can be forecast. Insufficient data were obtained during the summer of 1973 to provide a detailed statistical analysis of either track histories or

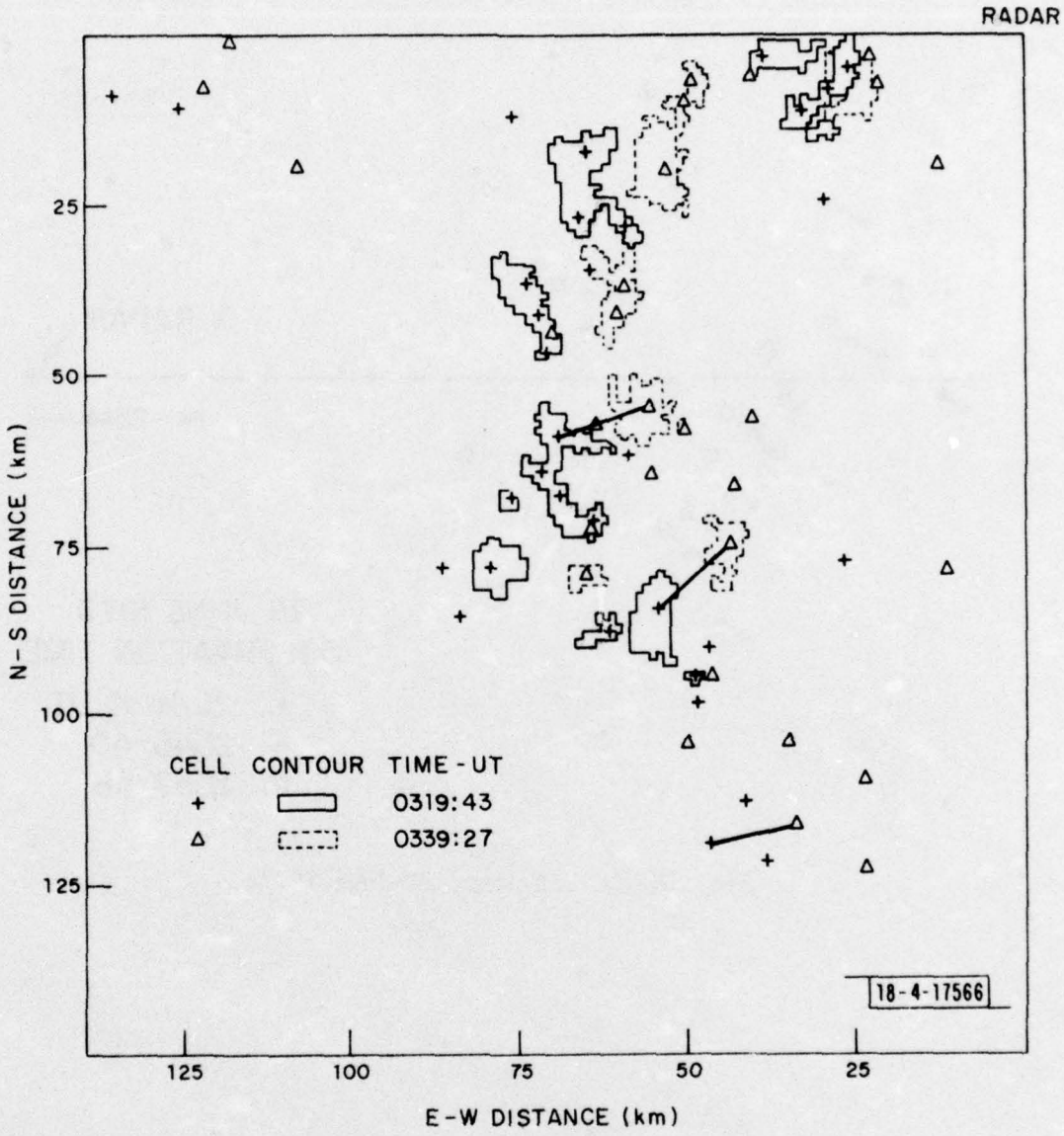

Fig. 17. Cell tracks, 14 August 1973.

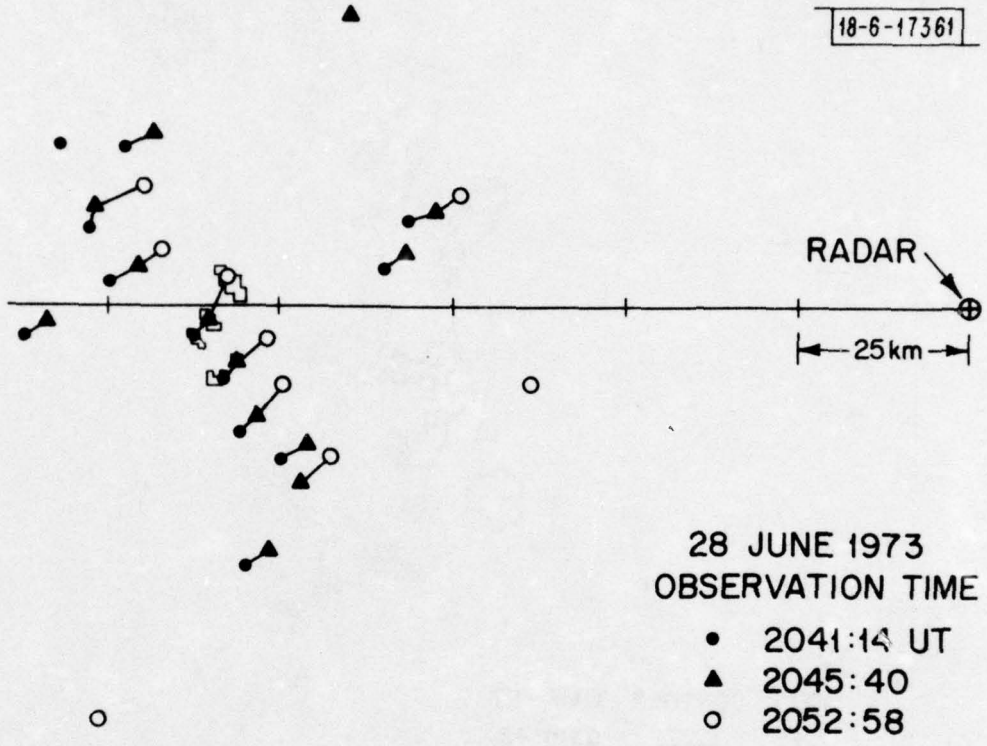

Fig. 18. Cell tracks, 28 June 1973.

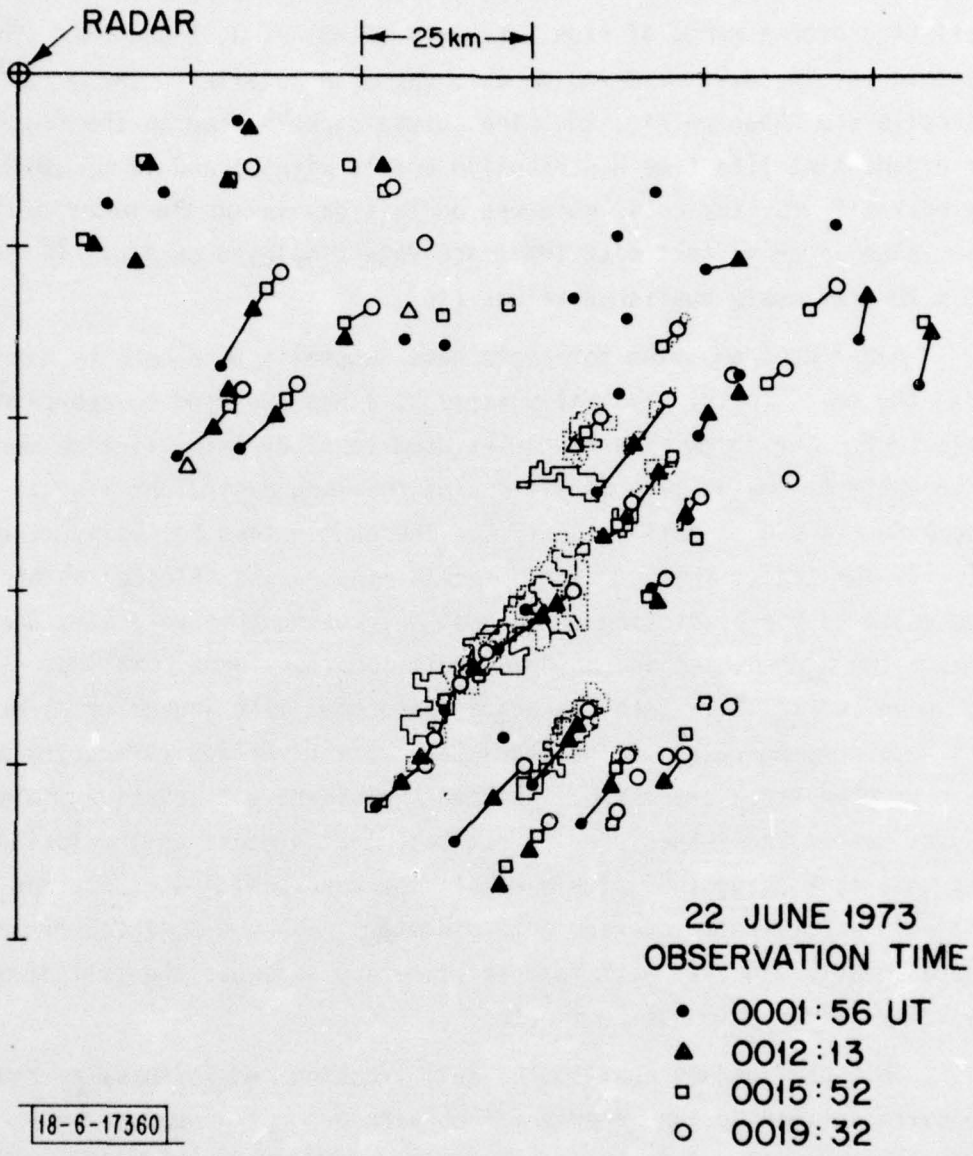

Fig. 19. Cell tracks, 22 June 1973.

forecast technique. For June 29, 1973, data were available to provide track statistics over a range of time intervals (Figs. 7, 8, 9 and 18). The time histories of 26 cells observed on this day were compiled. The persistence of the cells are shown on Fig. 20. The curves superimposed on the figure are for exponential life time distribution models with 11 and 14 minute half lives. The half life for the cells observed on this day is on the order of 12 minutes. This value is consistent with the track data displayed on Figs. 14 through 19 and with previously published values [16].

Radar echo position forecasts have generally been made by extrapolating along the cell tracks. Typically straight lines are used to approximate the trajectory. The track time histories used to study cell lifetime were also used to investigate the utility of extrapolating along a straight line as a forecast procedure. A single cell velocity was chosen for this analysis. The median velocity for tracks that persisted for 14 minutes was selected as the best estimate velocity for predicting cell location. Using this velocity, the differences between predicted and observed cell locations were compiled. The results are shown in Fig. 21. Both the average and root mean square (rms) deviation of positions perpendicular to the predicted track direction (traverse) and along the predicted track are shown. The mean values have a relative minimum at 14 minutes due to the method used to estimate the forecast cell velocity. The data show that using this simple model, the mean position errors for the cells were all less than the average cell diameter. The rms position errors increased nearly linearly with forecast time and exceeded the cell diameter in the traverse direction at 20 minutes.

This preliminary analysis of cell tracking and forecasting reveals that the cells defined by the algorithm for hazardous region detection persist and can be tracked. The cells have a lifetime on the order of 12 minutes for widespread and showery rain situations in the Virginia area. The cell trajectories tend to be curved and slightly different from each other requiring a forecast algorithm that establishes a best fit track for each cell and generates the forecast by extrapolation along that track. Due to the limited lifetime of the cells (except perhaps the most severe cells), consideration should be given

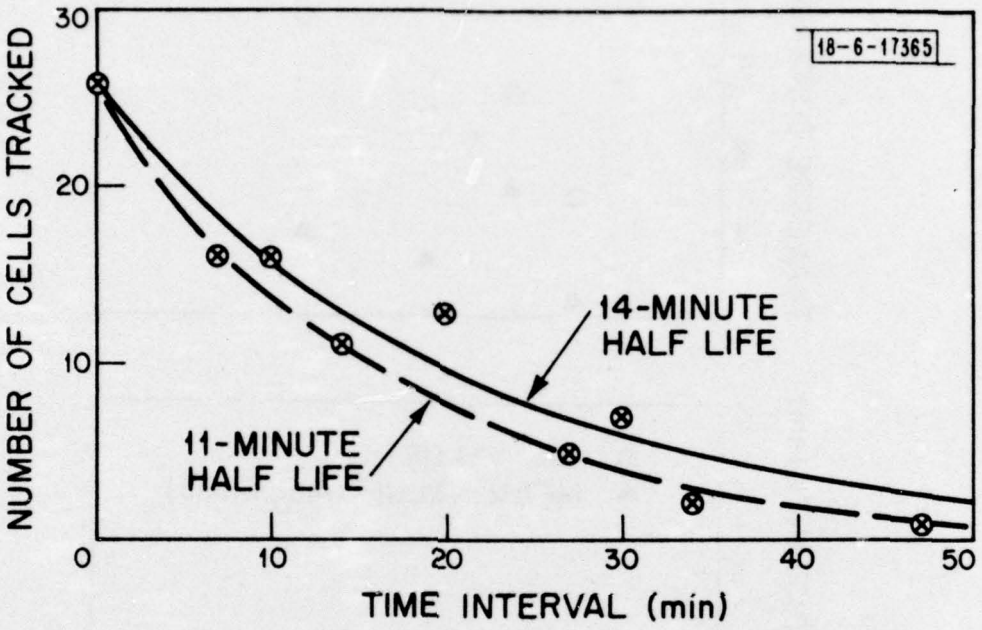

Fig. 20. Cell track life time, 29 June 1973.

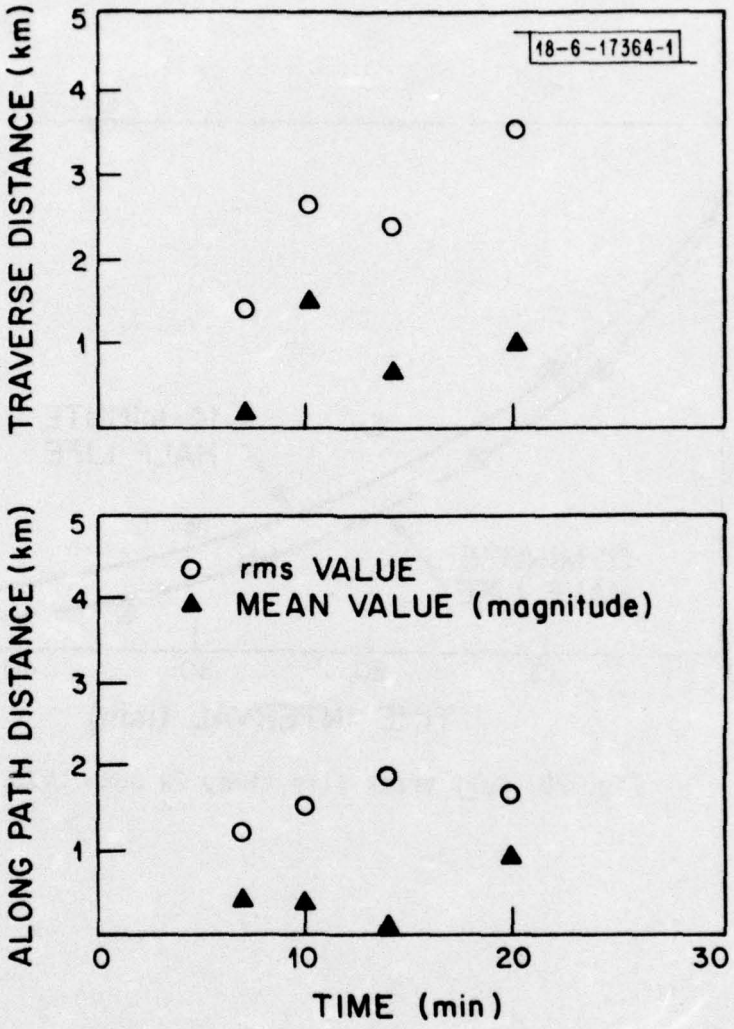

Fig. 21. Cell position forecast errors using a single cell velocity, 29 June 1973.

to predicting the sites for the development of new cells. New cell site prediction would also be useful for predicting the development of cells near the radar at heights above the radar beam (important out to 30 km from an ASR radar) before the rain falls into the beam. Cell development above the radar beam may delay cell detection by as much as 5 minutes depending upon the radar system, antenna scan pattern and range from the radar.

Radar observations made with a regular time spacing are required to forecast cell position. If 3 points are taken as the minimum required to provide an estimate of the cell trajectory prior to making an accurate forecast, then 2 to 3 minute spacings between observations are required to provide accurate predictions in the 10 to 20 minute time frame. Preliminary forecasts can be made when the cell is first detected based upon the behavior of other cells and those forecasts can be refined as successive cell detections are made. For long time periods between observations, most of the cells will have dissipated by the time refined forecasts can be made. Shortening the time separations between the 3 observations increases the error in estimating a cell trajectory because the cell translation will be small in comparison with the position uncertainty due to sampling error.

The tracking analysis presented above was based solely on cell position. Additional information can be obtained from the attributes of each cell. The intensities of the cells observed on Fig. 8 varied little from point to point along a track. Tracks 2, 6 and 7 had intensities that varied between 40 and 52 dB; tracks 1 and 5 had intensities that varied between 35 and 42 dBz. The cell attributes - intensity, area, and height can be used to help identify cells and possibly aid in estimating the extent of the hazard to be associated with each cell. Cell attribute data can also be used to determine the stage of cell development, whether the cell is growing or decaying, which should be useful in forecasting the severity of the hazard.

5.0 RADAR SYSTEM REQUIREMENTS

Successful application of the cell detection, tracking and forecasting scheme outlined above depends upon the adequacy of the radar data. The cell structure was readily apparent in the precise, small spatial resolution volume data available from the Millstone radar. More difficulty was encountered in interpreting the SPANDAR data due to the apparently decreased precision (larger sampling error) and in spite of the smaller spatial resolution volume. The data provided by NSSL was even less precise due to the limited number of samples used in generating a reflectivity estimate and only tentative estimates of cell location could be made. The quality of data currently collected from operational radars is even poorer (fewer independent samples).

Current operational radars can provide the required precision if coupled with a mini-computer system and operated in a way to provide more independent samples. The radar system requirements for successful application of the detection, tracking and forecasting scheme are given in Table I. Operational weather radars that operate at frequencies below 6 GHz and most of the surveillance radars in the FAA inventory can meet these requirements over a restricted operating range if they are suitably modified [3]. The requirements and their implications are discussed in detail below.

The radar system requirements listed in Table I are based on the results of the cell detection and tracking analysis described above. The average cell size is 2.9 km. Resolution element dimensions significantly smaller than the average size are wasteful of computer storage and processing time. Resolution elements larger than either the cell size or about one half of the smallest spacing expected between cells compromise the operation of the cell detection algorithms. Cell spacings are typically between 5 and 20 km (see Section 2.0 or [16]). The optimum resolution element size is thus between 1 and 3 km. The transverse resolution size is related to range and beamwidth. Antenna systems with beamwidths smaller than 1° are generally too large to be economical at the frequencies of interest. A 3 km transverse resolution size (1.6 nmi) is thus recommended. The recommended frequency

for a weather radar system [3] is in the 5 to 6 GHz range (C-band). Lower frequencies require larger antenna structures to provide the required beamwidth; higher frequencies suffer larger attenuations, due to propagation through the rain, that compromise the accuracy requirement.

A critical parameter in the operation of the cell detection algorithm is radar precision. Generally, the precision is limited by the statistical behavior of the scattered signal. A 0.5 dB rms sampling error requires between 64 and 128 independent samples depending upon the detection process used in acquiring the data [3]. Although radars often use this many samples in the integration process used for reflectivity estimation, the samples usually are not independent. To acquire a sufficient number of independent samples, the radar antenna must dwell at a fixed pointing angle or the data must be averaged over a number of scans. Single scan operation often requires one to two minutes per scan depending upon the number of independent range cells combined in a reflectivity estimate. To use the ASR/ARSR radars, multiple scan averaging will be required to provide a sufficient number of independent pulses at the higher rotation rates characteristic of surveillance radars. The pencil beam weather radars can obtain precise measurements on the lowest elevation angle scan to provide the precision required for cell detection and obtain data at higher elevation angles with less precision for use in estimating cell height. The higher elevation angle data can be obtained at a higher scan rate [3] to allow observations within the 2 to 3 minute spacings required to establish cell tracks. Observations can be made at different elevation angles during successive 2 to 3 mimute intervals to further refine the height data.

A 5 dB measurement accuracy is required to obtain intensity information for hazard estimation. The cell attributes -- height, intensity (reflectivity), and area -- appear to be related to the updraft velocity and cell age which should, in turn, be related to the intensity of the turbulence. One of the primary attributes used to judge severity and the possible existence of hail has been reflectivity. Reflectivity thresholds ranging from 35 to

55 dBz have been suggested as a measure of storm severity and hail occurrence. Figure 9 shows that significant increases in the number of possibly hazardous cells occur with each 5 dB decrease in reflectivity value. Some of the uncertainty in the association of reflectivity with hazard has been in the inaccuracies of the radars used in making observations. Keeping the total measurement accuracy to less than 5 dB reduces the number of cells erroneously labeled as hazardous. Several sources of measurement inaccuracy exist: calibration error (includes sensitivity changes, etc.), attenuation, beamfilling, and polarization mismatch. All radar systems have calibration errors and a reasonable goal for an operational radar system is 4 dB. The error to be attributed to attenuation, beamfilling, and polarization mismatch is 3 dB. Using root sum of squares for combining measurement errors results in the 5 dB accuracy.

Polarization mismatch is only important for the ASR/ARSR radars and only when circular polarization is used to reduce rain clutter. Ideally, with spherical rain drops and an antenna that responds only to the transmitted sense circular polarization, rain should not be detectable. In practice, antennas are not perfect and hydrometers are not spheres. The integrated cancellation ratio, and hence the apparent reflectivity, varies as a function of storm type and true reflectivity. The ASR/ARSR radar cannot satisfy the accuracy requirement at any range if circular polarization is used unless an orthogonal sense circular polarization channel is provided. The surveillance radar can meet the requirements for hazard detection if either an orthogonal circular polarization receiver channel is used when circular polarization is transmitted, or only linear polarization is used [3].

Beamfilling refers to the measurement errors produced by cells that do not fill the resolution volume. By selecting the azimuth beamwidth such that the transverse resolution requirement is met, beamfilling will not be a problem in the horizontal. Surveillance radars have fan shaped beams with vertical (elevation) beamwidth several times larger than the horizontal (azimuth) beamwidth. Cells that are not high enough to fill the beam will be reported

as having a reduced reflectivity. Using a 3.5 km (11.5 kft) cell as a standard for calculating the effect of beamfilling, the maximum range values for meeting the 3 dB portion of the accuracy requirement can be estimated. The maximum range for a 4.8° elevation pattern in the ASR radar is 75 km (40 n.mi); the maximum range for the 2° beamwidth WSR-57 is 136 km (73 n. mi); the maximum range for a 1.6° beamwidth C-band radar is 155 km (84 n. mi); and the maximum range for the 1° beamwidth recommended in [3] as a joint use FAA, NWS and AWS weather radar is 180 km (97 n. mi).

Attenuation by rain along the path between the radar and the rain cell can cause additional measurement error. A 3 km, 45 dBz cell introduces a 0.1 dB measurement error at S-band and a 0.7 dB measurement error at C-band. The difficulty with using the higher frequency for measurements is that significant attenuation (compared to 3 dB) can occur for measurements made lengthwise through a squall line with a number of intense cells (> 55 dBz). This problem could be overcome with more than one radar for observations and selecting the highest of the observed reflectivity values. If hail were not present, precise and accurate reflectivity measurements can be used to estimate the attendant attenuation that occurred along the path. This technique only works when both the accuracy and precision errors are small. The detrimental effect of attenuation at C band is more than offset by the horizontal and vertical beamfilling errors that occur at S-band when the beamwidth is too large. Thus C band is recommended.

The update rate requirement is based upon the desire to obtain three position estimates within a 5 to 6 minute period to provide a trajectory estimate for extrapolation to produce an accurate forecast. If an additional 1 to 2 minute interval is added to the time interval required for observation to account for processing, distribution and display, the accurate forecast data reaches the controller 6 to 8 minutes after first detection.* This value

*The controller receives a forecast with the first cell detection. This forecast is improved by the 2nd and 3rd observation and is nearly optimized in 6 to 8 minutes after first detection.

is a significant fraction of the half life of a cell and intervals larger than 2 to 3 minutes between observations cannot be tolerated. Shortening the time separations between the 3 observations increases the error because the cell translation will be small in comparison with the position uncertainty due to sampling errors and the transverse resolution element size.

Most radars can meet the time requirements if suitably modified. Pencil beam weather radars can meet the update rate requirement, the precision requirement, and obtain height information if two scan types are used. Precision measurements can be made at the lowest elevation angle using a slow antenna scan rate and less precise measurements can be made at higher elevation angles using higher scan rates. Modifications required for operational weather radars include both the addition of digital processing and restrictions against the manual scanning operations currently used for determining the cell tops and cell motion. Cell tops and motion will be automatically obtained by the digital processor using raster scan data.

The processing algorithms demand digitized radar data and accompanying data processing facilities. A mini-computer will be a required element in each weather radar system [3]. In addition to the data preparation and cell detection chores, the processor should also be used to remove ground clutter. The ground clutter must be automatically rejected to provide reliable and readily interpretable data to the controllers. Two levels of processing are required for ground clutter suppression: one using information on average Doppler (coherent) and/or Doppler spread (coherent or noncoherent) obtained while generating reflectivity estimates and the second using detected cell track velocities. Both levels are required, the first to discriminate between weather echoes and ground clutter prior to the cell detection processor and the second to eliminate stationary cells due to ground clutter [3].

Table I summarizes the radar system requirements described above. A number of radars currently available in the FAA, NWS, and U.S. Air Force inventory are capable of meeting these requirements with the addition of digital data processing equipment and, for the ASR radars, an orthogonal

circular polarization channel. When suitably modified, the available radars are useful to a maximum range imposed by the accuracy and transverse resolution requirements. The maximum ranges are fixed by the antenna beamwidths. A 1° beam radar system is recommended for use in the en route environment to provide weather surveillance over the widest possible area with the least number of radars. For joint use with the NWS and U.S. Air Force, the radar requirements listed in Table I will be little changed except for, possibly, a higher accuracy requirement. The 5 dB accuracy requirement translates to a factor of 2 measurement accuracy for rain rate and liquid water content. For hydrological applications, higher accuracies may be required. In all other respects, the requirements listed here should be compatible with other demands on the radar system.

6.0 CONCLUSIONS AND RECOMMENDATIONS

The investigations reported herein have yielded results and conclusions as follows:

A. A procedure has been advanced for radar detection of convective turbulence regions potentially hazardous to aviation which centers about detection of radar reflectivity maxima (called cells). This procedure is based on both physical reasoning and a limited set of simultaneous radar observations and aircraft storm penetrations. Moreover, this detection technique has been shown to be compatible with feasible very short term forecasts (i.e., a few tens of minutes) of cell position needed for air traffic control [1].

B. Required radar system characteristics for both depiction and forecasting of individual cells have been identified (Table 1). The practical achievement of these characteristics is established in the companion volume [3]. Details of the ASR modifications to satisfy terminal requirements and weather radar designs to satisfy en route applications are described therein.

C. A preliminary investigation of Doppler techniques revealed that practical limitation on radar beamwidth and operating range hinders direct observation of turbulence on the scale size of 50-300 meters which is of principal concern to aviation. Unfortunately, no reliable correlation has been established between turbulence hazardous to aircraft and the scale size of data measured by typical radar (e.g., 1-2 km resolution at 10 km from the radar).

Further refinement in techniques for depiction and forecasting should center about:

A. Full statistical verification and refinement of the depiction and forecasting algorithms employing additional aircraft penetration, and simultaneous, high precision, high update rate radar reflectivity measurements.

B. Investigations focused on extracting the most relevant data from both reflectivity and Doppler data to yield more nearly optimized hazardous cell depiction and forecasting procedures.

C. Study of the organization of convective cells and the extent to which the location of new cells may be predicted before the cells develop.

APPENDIX

USE OF DOPPLER RADAR

Studies of turbulence in and around clouds have shown that turbulence is more strongly developed inside clouds, particularly cumulus clouds, and most especially cumulonimbus (thunderstorm) clouds [7]. The wind field responsible for turbulence in a cloud system is often considered on two scales: the small mesoscale currents or streams that occur with 1 to 20 km dimensions (the draft described in the Thunderstorm Project Report [4]) and the smaller scale size fluctuations described as turbulence (gusts [4]).

Figure 1 provides a schematic view of the small mesoscale currents (up and down drafts) within a mature cumulonimbus cloud. Instrumented aircraft traverses through thunderstorms reveal velocity fluctuations on a wide range of scale sizes. Figure A1 (adapted from Sinclair [A1]) depicts the spatial vertical velocity fluctuation within thunderstorms with 50 to 60 dBz peak reflectivities at heights between 4.5 and 10 km MSL (15 to 33 dft) in Oklahoma and Colorado. The one dimensional spatial spectra shown in Fig. A1 were calculated from temporal fluctuations of vertical velocity measured on horizontal aircraft passes through storm cores and are reported as spatial fluctuations using the aircraft velocity and assuming that the wind field did not change during a traverse. Each spectrum was positioned on the figure to coincide with the $\kappa^{-5/3}$ line at high wavenumbers. Turbulence in the free atmosphere is generated at large scale sizes and is dissipated by molecular action at very small scale sizes [A2, A3]. The wavenumber region separating the generation and dissipation regions is modeled to have a $\kappa^{-5/3}$ behavior and is called the inertial subrange. The turbulent fluctuations depicted in Fig. A1 were generated at scale sizes in excess of 200 to 2,000 m (700 to 7,000 ft) -- scales at which the measured spectra depart from the $\kappa^{-5/3}$ line -- and dissipated at scale sizes less than 10 m (30 ft). Note the departure, in Fig. A2, of these measured curves from the often modeled $\kappa^{-5/3}$ line demonstrating a poor correlation between spectral levels at significantly different scale sizes, e.g., wavenumbers of 1 and 100.

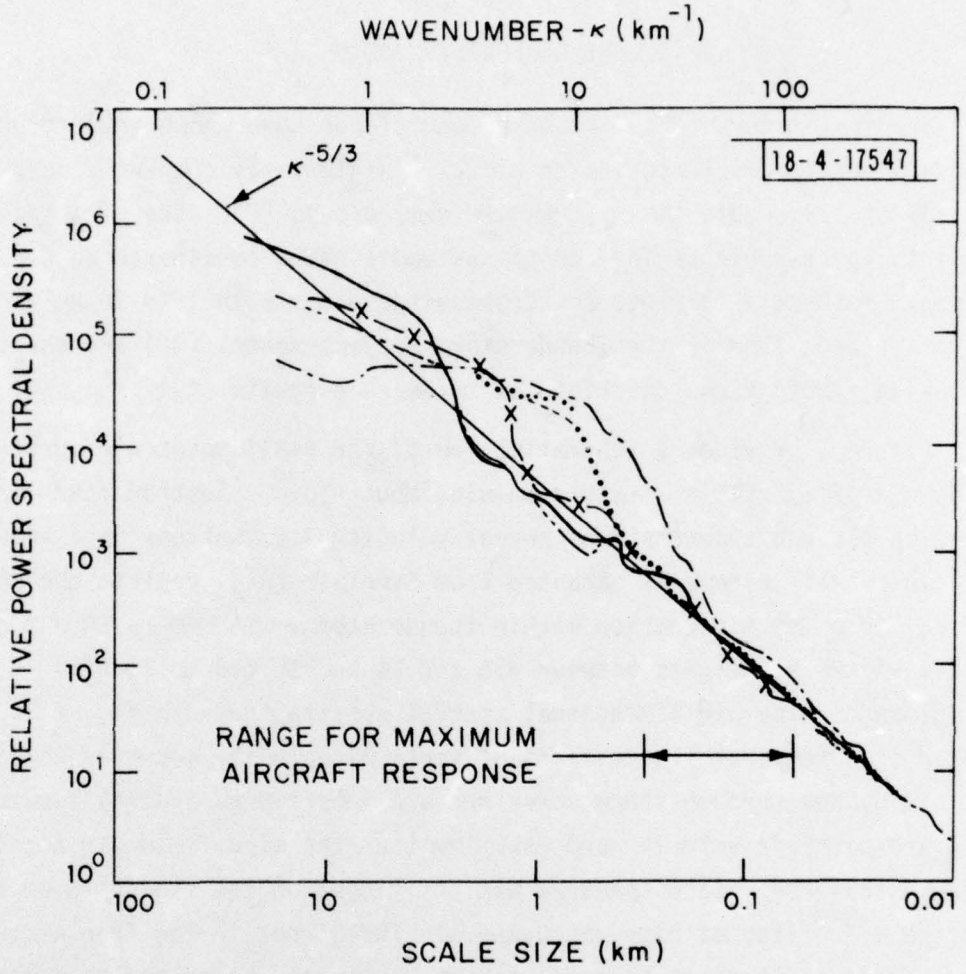

Fig. A1. Power spectra of vertical velocity fluctuations obtained within thunderstorms (adapted from Sinclair [A1]).

The turbulent bumps (accelerations) experienced by aircraft are caused by vertical velocity fluctuations in the 60 to 300 m (200 to 1,000 ft) scale size range. Larger scale size fluctuations cause systematic changes in altitude without fluctuations in pitch, roll, and yaw and are not hazardous except for possible inadvertent pilot or control system response to the unexpected change. Aircraft do not respond to smaller scale fluctuations. In recognition of the limited scale size range responsible for turbulence as experienced by aircraft, encounters with turbulence are usually studied using discrete gust analysis [A4]. Discrete gust analysis predicts the response of different aircraft to a given realization of a turbulent wind field. The response of an aircraft to turbulence is modeled by assuming that the turbulent vertical velocity fluctuations can be represented by a number of discrete isolated gusts of fixed horizontal dimension and of variable intensity. The horizontal scale length of the hypothetical gust varies with aircraft design, is specified in units of the aircraft wing chord length, and typically ranges from 60 to 300 m. for current commercial aircraft. A derived gust velocity is used to specify the intensity of the isolated gust. For a given aircraft design, the vertical acceleration can be calculated from the derived gust velocity when the weight, altitude, and speed of the aircraft is known. Using the concept of hypothetical isolated gusts, accelerations measured by one aircraft may be used to calculate the expected vertical accelerations of another flying through the same field of turbulence.

Remote means for estimating the turbulent energy (eddy) dissipation rate (a measure of the rms wind fluctuations for a limited range of scale sizes within the inertial subrange [A2, A3]) are required for the assessment and forecast of aircraft hazard. Unfortunately, at the current time, only direct, in-situ aircraft measurements can provide the data at the required scale sizes. Doppler radars have the potential for providing remote observations of turbulence within a volume containing rain. Due to pulse volume averaging, radar observations of either reflectivity variations or of Doppler spread are generally made at scale sizes associated with the production

of turbulence (greater than 2 km*) and cannot be used to provide direct measurements of turbulence in the inertial subrange. For a 1° beamwidth the transverse resolution element size exceeds 200 m at distances greater than 11.5 km from the radar. Direct observations of inertial subrange turbulence can only be made at distances less than 11.5 km using Doppler spread and a 1° beamwidth antenna system. Direct observations may be possible at longer ranges using a 1° beamwidth system and analyzing the shape of the Doppler spectrum. To date, no attempt has been made to systematically analyze Doppler spectra.

Scanning radar measurements of Doppler spread are dominated by the production region variance. They are an indicator of mesoscale wind shear (primarily of horizontal velocities at the low elevation angles typically employed for radar observations) rather than aircraft turbulence because of the poor correlation exemplified in Fig. A1. A sample of Doppler spread and simultaneous aircraft penetration observations obtained by NSSL in Norman, Oklahoma, points this out [13]. Figure A2 displays Doppler spread and aircraft observations of turbulence made at ranges between 145 and 154 km (~90 st.mi) from the Doppler radar at Norman. At these ranges, the 1° radar beam spans 2.5 km (1.6 st. mi) in both the horizontal and vertical dimensions transverse to the pointing direction of the radar. Doppler spread data are shown only for regions with reflectivity values in excess of 30 dBz and for two or more observations out of 9 possible observations at the same location with spread values greater than or equal to 7 and 10 m/s (23 and 30 ft/s).

The thresholds displayed are commensurate with the rms values identified as a threshold for cumulus cloud turbulence by Steiner and Rhyne [A4]. The Doppler spread radar measurements are dominated by fluctuations at the largest scale size within the resolution volume. If their one dimensional spectrum had a true $\kappa^{-5/3}$ behavior, the radar observed variances would be roughly an

*Since the Doppler spread measurements approximate an integral of the total energy from below 2 km on a spatial scale, the resultant value is dominated by energy outside the turbulent region.

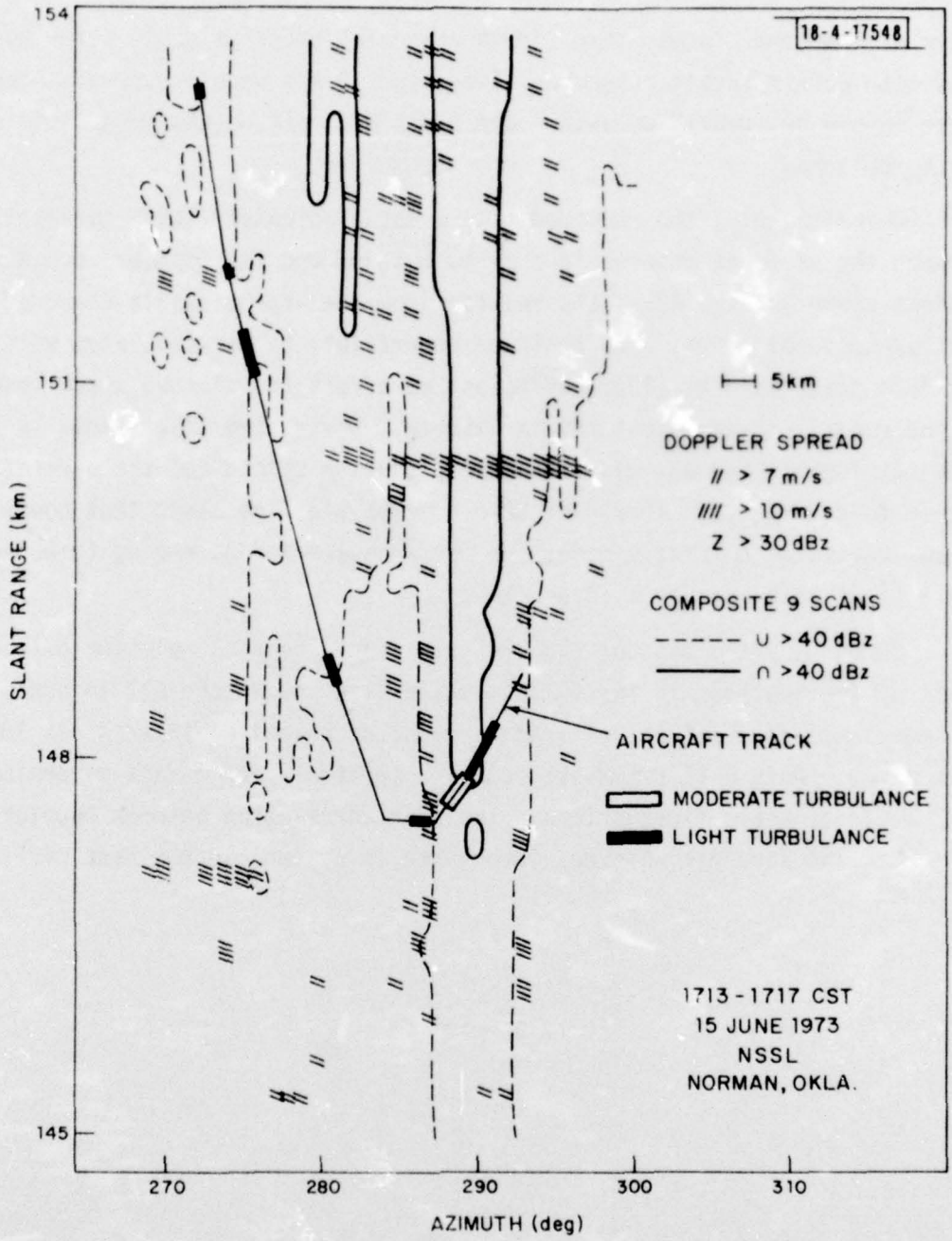

Fig. A2. Doppler spread observations and aircraft turbulence in a thunderstorm.

order of magnitude larger than for the inertial subrange scale sizes associated with peak aircraft response. The 7 and 10 m/s Doppler spread thresholds there should be identified with 2 and 3 m/s aircraft observation, sufficient for turbulence.

Unfortunately, the recorded flight data indicates little correlation between the aircraft observations of turbulence and the Doppler spread observations shown in Fig. A2. This results from the unpredictable shape of the spatial spectral curve. The position uncertainty to be associated with the aircraft track is 1 km [13], sufficient to affect the plotted track location in the radial direction but not in azimuth. Moving the track radially by 1 km does not improve the association between Doppler spread and the aircraft response to turbulence. Thus, the data corroborates the claim that Doppler spread measurements, as currently made, are not adequate for observing turbulence on scale sizes that present a hazard to aircraft.

In summary the data of Fig. 1A evidences a poor correlation between vertical fluctuations in the 1-10 km scale size and in the 0.1 km scale size of importance to aviation. At radar ranges of practical interest (> 10 km from a radar with a 1° beamwidth) Doppler spectral spread data is dominated by the larger scale fluctuations. The poor correlation between Doppler spectral data and aircraft measured turbulence is evident in the data of Fig. A2.

REFERENCES

1. S.I. Krich and S.M. Sussman, "A Concept and Plan for the Development of a Weather Support Subsystem for Air Traffic Control, Project Report ATC-64, Lincoln Laboratory, M.I.T. (16 April 1976).

2. L.J. Battan, Radar Observation of the Atmosphere, University of Chicago Press, Chicago (1973).

3. S.M. Sussman "Radar Detection of Thunderstorm Hazards for Air Traffic Control, Volume: II Radar Systems," Project Report ATC-67, Vol. II, Lincoln Laboratory, M.I.T. (7 October 1976).

4. H.R. Byers and R.R. Braham, The Thunderstorm - Report of the Thunderstorm Project, Ch. 9 and 10, U.S. Dept. of Commerce, Weather Bureau, Washington, D.C. (June 1949).

5. J. Burnham and J.T. Lee, "Thunderstorm Turbulence and Its Relationship to Weather Radar Echos," J. Aircraft, 6, 438-445 (1969).

6. J.T. Lee, "Thunderstorm Turbulence Concurrent Doppler Radar and Aircraft Observations 1973," Preprints 6th Conf. on Aerospace and Aeron. Meteorol., pp. 295-298, Amer. Meteorol. Soc., Boston (November 1974).

7. N.K. Vinnichenko, N.Z. Pinus, S.M. Shmeter, and G.N. Shur, Turbulence in the Free Atmosphere, Ch. 8, Hydrometeorological Press, Leningrad (1968). (Translation available from Consultants Bureau, New York, 1973).

8. B.J. Mason, The Physics of Clouds, 2nd Edition, Ch. 6, Clarendon Press, Oxford (1971).

9. R.A. Kropfli and L.J. Miller, "Thunderstorm Flow Patterns in Three Dimensions from Dual-Doppler Radar," Preprints 16th Radar Meteorol. Conf., pp. 121-217, Amer. Meteorol. Soc., Boston (April 1975).

10. A.A. Chernikov, A.A. Ivanov, and Y.V. Melinichuk, "The Turbulence Structure in Cumulonimbus Clouds," Preprints Conf., pp. 134-137, Amer. Meteorol. Soc., Boston (April 1975).

11. R.K. Crane, "Bistatic Scatter from Rain," IEEE Trans. Antennas and Propagation, AP-22, 312-320 (1974).

12. J.S. Marshall and W. Hitschfeld, "Interpretation of the Fluctuating Echo from Randomly Distributed Scatterers, Part I," Can. J. Phys., 31, 962-994 (1953).

13. Data sample provided by J.T. Lee of the National Severe Storm Laboratory, Norman, Oklahoma.

14. I. Katz, A. Arnold, J. Goldhirsch, T.G. Konrad, W.L. Vann, E.B. Dobson, and J.R. Rowland, "Radar Derived Spatial Statistics of Summer Rain," NASA CR-2592, Vol. I, NASA Washington, D.C. September 1975).

15. R.K. Crane, "Virginia Precipitation Scatter Experiment - Data Analysis," NASA/GSFC X-750-73-55, NASA Goddard Space Flight Center, Greenbelt, MD (November 1972).

16. P.M. Austin and R.A. Houze, Jr., "Analysis of Mesoscale Precipitation Areas," preprints 14th Radar Meteorol. Conf., pp. 329-334, Amer. Meteorol. Soc., Boston (November 1970).

A1. P.C. Sinclair, "Severe Storm Turbulence Energy Structure," Unpublished presentation at the 6th Conf. on Aerospace and Aeron. Meteorol., Amer. Meteorol. Soc. (November 1974).

A2. J.L. Lumley and H.A. Panovsky, The Structure of Atmospheric Turbulence, Interscience Publishers, New York (1964).

A3. A.S. Monin and A.N. Yaglom, Statistical Fluid Mechanics, Vol. 2, Ch. 7 and 8, M.I.T. Press, Cambridge (1975).

A4. R. Steiner and R.H. Rhyne, "Some Measured Characteristics of Severe Storm Turbulence," National Severe Storms Project Report No. 10, U.S. Dept. of Commerce, Weather Bureau, Washington, D.C. (July 1962).